Winter Mixed Layer Development in the Central Irminger Sea: The Effect of Strong, Intermittent Wind Events

KJETIL VÅGE AND ROBERT S. PICKART

Woods Hole Oceanographic Institution, Woods Hole, Massachusetts

G. W. K. MOORE

University of Toronto, Toronto, Ontario, Canada

MADS HVID RIBERGAARD

Danish Meteorological Institute, Copenhagen, Denmark

(Manuscript received 11 August 2006, in final form 21 May 2007)

ABSTRACT

The impact of the Greenland tip jet on the wintertime mixed layer of the southwest Irminger Sea is investigated using in situ moored profiler data and a variety of atmospheric datasets. The mixed layer was observed to reach 400 m in the spring of 2003 and 300 m in the spring of 2004. Both of these winters were mild and characterized by a low North Atlantic Oscillation (NAO) index. A typical tip jet event is associated with a low pressure system that is advected by upper-level steering currents into the region east of Cape Farewell and interacts with the high topography of southern Greenland. Heat flux time series for the mooring site were constructed that include the enhancing influence of the tip jet events. This was used to force a one-dimensional mixed layer model, which was able to reproduce the observed envelope of mixed layer deepening in both winters. The deeper mixed layer of the first winter was largely due to a higher number of robust tip jet events, which in turn was caused by the steering currents focusing more storms adjacent to southern Greenland. Application of the mixed layer model to the winter of 1994–95, a period characterized by a high-NAO index, resulted in convection exceeding 1700 m. This prediction is consistent with hydrographic data collected in summer 1995, supporting the notion that deep convection can occur in the Irminger Sea during strong winters.

1. Introduction

Deep convection in the open ocean occurs when a unique set of oceanic and atmospheric conditions are satisfied. This includes strong atmospheric forcing, a sufficiently preconditioned water column, and cyclonic circulation that isolates the water parcels (Marshall and Schott 1999). Consequently, there are only a limited number of locations in the World Ocean where deep overturning occurs. One such site is the Labrador Sea, where the intermediate water mass known as Labrador Sea Water (LSW) originates. Formation of LSW via deep convection has important consequences for the North Atlantic meridional overturning circulation (Schmitz and McCartney 1993), for the global heat budget (Talley 2003), for the modification of the dense overflow waters from the Nordic Seas (McCartney 1992; Dickson and Brown 1994), and for the stratification and ventilation of the interior North Atlantic (Pickart et al. 2002). Recently it has been argued that LSW is also formed by deep convection in the southwest Irminger Sea (e.g., Pickart et al. 2003a,b; Straneo et al. 2003; Bacon et al. 2003; Falina et al. 2007). If this is true, it will likely have similar consequences, and also influence the biological productivity in the region (Sverdrup et al. 1942) as well as the spreading of LSW into the North Atlantic (Sy et al. 1997). It is therefore important that we understand the factors governing the seasonal deepening of the mixed layer in the Irminger Sea, which appear to be different from the conditions leading to convection in the Labrador Sea.

Corresponding author address: Kjetil Våge, Woods Hole Oceanographic Institution, Woods Hole, MA 02543.
E-mail: kjetil@whoi.edu

DOI: 10.1175/2007JPO3678.1

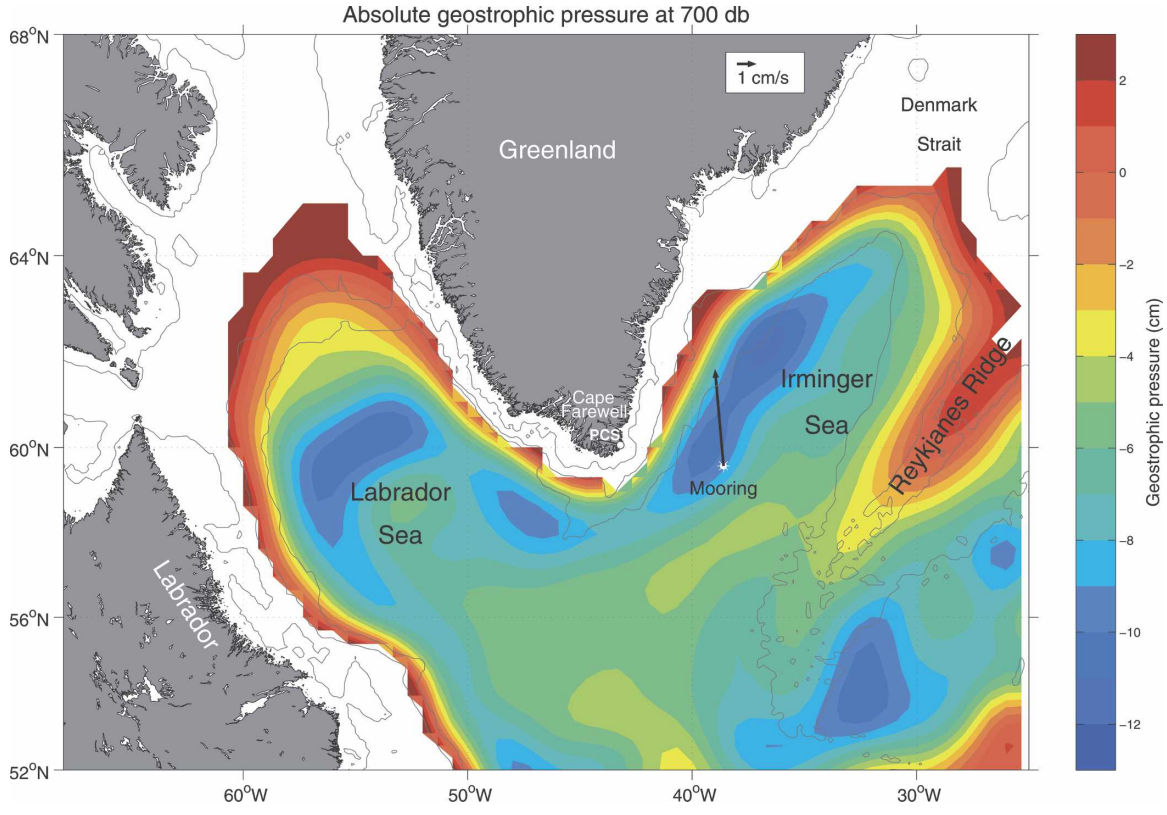

FIG. 1. Objectively mapped absolute geostrophic pressure at 700 db, from Lavender et al. (2000). A series of cyclonic recirculations (associated with low geostrophic pressure) are located in the Irminger and Labrador Seas. The mooring position is indicated by the white star, and the mean current vector at 700 db for 2002–04 is shown. The isobaths (gray lines) are 200, 1500, and 2500 m. The location of the Prins Christian Sund coastal meteorological station is indicated by PCS.

In the North Atlantic, low pressure systems following the winter storm track advect cold, dry continental air from the Canadian landmass over the southwestern Labrador Sea (Fig. 1), where convection has been observed to reach 2 km (Clarke and Gascard 1983; Lilly et al. 1999; Pickart et al. 2002). Large heat fluxes result when the air reaches the ice-free ocean (Lab Sea Group 1998; Moore and Renfrew 2002). The retention of water from the previous winters' deep convection provides a preconditioned state (Marshall and Schott 1999; Lazier et al. 2002), and a localized cyclonic recirculation gyre in the western Labrador Sea (Lavender et al. 2000) isolates the water resulting in exposure to the atmospheric cooling for an extended period of time. The LSW formed is characterized by low salinity and a lower potential vorticity (PV)[1] than any other water mass in the North Atlantic (Talley and McCartney 1982). The production and characteristics of LSW exhibit significant interannual variability (Talley and McCartney 1982; Lazier et al. 2002), which is correlated with the North Atlantic Oscillation (NAO; Dickson et al. 1996).

One of the pieces of evidence suggesting that LSW is also formed in the Irminger Sea involves the distribution of tracers. A lateral map of the middepth distribution of PV from data collected during the high-NAO period of the early 1990s shows a second, isolated minimum in the Irminger Sea (Pickart et al. 2003a). The spreading of LSW was investigated with advective–diffusive models (Straneo et al. 2003; Kvaleberg et al. 2007, manuscript submitted to *J. Geophys. Res.*), and the results imply that the Irminger Sea is associated with a local source of low-PV water. Pickart et al. (2003a) showed that, similar to the Labrador Sea, the conditions for deep convection are satisfied in the Irminger Sea except for the atmospheric forcing. The heat flux events associated with the passage of synoptic-scale low pressure systems are up to 30% smaller, since Greenland represents a smaller reservoir of cold, dry continental air than Canada and most of the air reach-

[1] Planetary potential vorticity is defined as $\mathrm{PV} = (f/\rho)(\partial\rho/\partial z)$, where f is the Coriolis parameter, ρ is density, and z is depth.

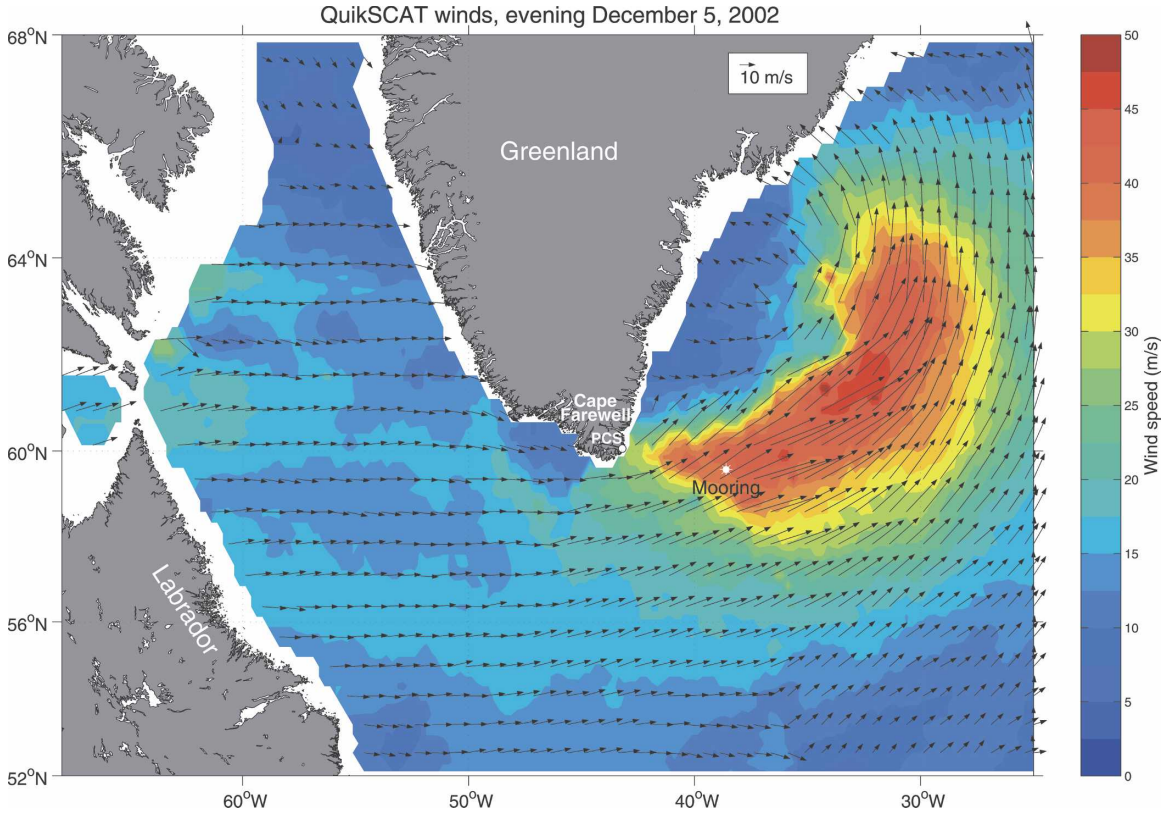

FIG. 2. The QuikSCAT wind speed (color) and vectors (every ninth point) showing a tip jet on 5 Dec 2002. The wind speed at the mooring site (white star) during this event was 37 m s^{-1}.

ing the Irminger Sea has already been modified by the Labrador Sea.

The analysis carried out by Pickart et al. (2003a) was based on the relatively low-spatial resolution National Centers for Environmental Prediction (NCEP) reanalysis fields (Kalnay et al. 1996). A mechanism capable of enhancing the heat fluxes over the southern Irminger Sea exists in the form of a strong but narrow and intermittent wind pattern called the Greenland tip jet (Doyle and Shapiro 1999; Pickart et al. 2003b), which is not properly resolved by NCEP. Tip jets are predominantly a wintertime phenomenon formed in the lee (eastern) side of Cape Farewell. They are triggered by low pressure systems that enter the region northeast of Cape Farewell, and they occur more often during high-NAO winters when the storm track is shifted northeastward (Moore 2003). Recently it has been argued that the latitude of the center of the Icelandic Low is more strongly related to the occurrence of tip jet events than the sea level pressure (SLP) signal of the NAO (Bakalian et al. 2007).

Even though tip jet events are intermittent and seasonal, their signature is evident in a 4-yr average of wind stress curl (Chelton et al. 2004). This positive curl is important for the regional circulation and possible deep convection in the Irminger Sea (Spall and Pickart 2003; Pickart et al. 2003a). Figure 2 shows a typical tip jet as it appears in the high-resolution data from the SeaWinds microwave scatterometer on the Quick Scatterometer (QuikSCAT) satellite. The upper limit of the scatterometer winds (50 m s^{-1}) was reached during this event, while the greatest registered NCEP wind speed for the same event was 24 m s^{-1}, less than half the QuikSCAT value. QuikSCAT data were first applied to the study of tip jets by Moore and Renfrew (2005). The high wind speeds, low temperature, and relatively low humidities characteristic of tip jet events are readily detected using data from a meteorological station situated adjacent to Prins Christian Sund (PCS) near Cape Farewell (Pickart et al. 2003b; see Fig. 2).

The goals of the present study are to examine the development of the winter mixed layer in the central Irminger Sea, assess the importance of the Greenland tip jet in driving convection, and investigate the atmospheric conditions that lead to tip jet events. To accomplish this we use in situ data from a moored profiler deployed east of Cape Farewell, along with a variety of atmospheric datasets. A description of the moored pro-

filer data and properties of the mixed layer are presented first, followed by an investigation of the wintertime atmospheric conditions over the southwest Irminger Sea in general and during tip jet events in particular. These results are then used to develop an improved estimate of the heat flux time series at the mooring site, which in turn is used to force a one-dimensional mixed layer model of the overturning.

2. Moored profiler data

In 2001 a field program was initiated to obtain direct winter season observations of the water column in the southwest Irminger Sea using a moored profiler (MP; Doherty et al. 1999) positioned in the center of the minimum PV region east of Cape Farewell, under the expected path of the Greenland tip jet (Figs. 1 and 2). The MP was equipped with a conductivity–temperature–depth (CTD) sensor and an acoustic current meter (ACM), and was programmed to obtain twice-daily profiles between 60 and 1800 m. The mooring also contained a vector averaging current meter (VACM) and thermistor, located below the profiler at 1840 m.

The MP failed shortly after the first deployment, but the second deployment returned 582 profiles between early August 2002 and early June 2003, and the third deployment resulted in 471 profiles between early August 2003 and late March 2004. During the remainder of this study, the 2002–03 (abbreviated 0203) and 2003–04 (abbreviated 0304) deployments will be referred to as the first and second deployments, respectively. Ascending profiles started at 0000 UTC and descending profiles started at 0600 UTC. Each profile took about 2 h to complete. When not profiling, the MP rested in stand-by mode at the top and bottom of the profiling range. During the course of each deployment, the profiler started drifting slowly while in stand-by mode toward its neutrally buoyant position at middepth. This tendency became more pronounced with time, yielding as a result essentially one full profile per day toward the end of the period.

The raw CTD and ACM data were filtered, despiked, and averaged into 2-db pressure bins (Toole et al. 1999). Shipboard CTD casts were carried out at the mooring site after deployment and prior to recovery for calibration purposes (11 August 2002, 30 July 2003, and 24 July 2004). The first CTD cast was given the most weight because of the premature termination of the deployments. Conductivity drift and offset were determined by requiring the mean potential conductivity ratio of the MP and the shipboard CTD to be the same in the depth interval where the temperature–salinity relation was most stable. This interval was located below the previously formed LSW (i.e., formed during the 1990s), near 1100–1200 db. Below the mixed layer a stable stratification was assumed, and interpolations were performed over density inversions exceeding 0.005 kg m^{-3}. This threshold was determined from a consideration of the range of density variability in the above mentioned interval of stable temperature–salinity characteristics. Less than 30% of the profiles in each deployment contained inversions, and most were caused by outliers missed by the despiking routine. The ACM data were corrected for a bias related to change in impedance of the circuit connecting the acoustic transducers to the current meter electronics with pressure (J. Toole 2005, personal communication) and adjusted to take into account the pressure dependency on the speed of sound, and then matched to the VACM record. The resulting measurement uncertainties were estimated to be 0.004 for salinity, 0.005°C for temperature, 2 cm s^{-1} for current speed, and 30° and 45° for current direction for the first and second deployments, respectively. The reader is referred to Våge (2006) for details of the calibration procedure and accuracy estimates.

3. Properties of the mixed layer

The calibrated data from the MP CTD were used to derive the potential temperature (θ) and potential density (σ_θ), referenced to the sea surface, and the buoyancy frequency (N). These quantities were smoothed and uniformly gridded (10 m in depth and 12 h in time) to make property–time plots. The results are displayed in Figs. 3 and 4. Among the most noticeable features is the signature of the deepening mixed layer in the salinity and buoyancy frequency plots. The enhancement of the buoyancy frequency at the base of the mixed layer is caused by the large vertical density gradient where the mixed layer density profile joins the underlying part of the profile. As winter progresses and the mixed layer deepens, the gradient at the base of the mixed layer decreases because of the less abrupt transition to the remainder of the profile; hence this feature of the buoyancy frequency becomes less effective as an indicator of mixed layer depth in late winter (Våge 2006).

The previously formed ambient LSW layer is recognizable by the salinity minimum and the local minimum in buoyancy frequency, which like PV indicates weak stratification, centered around 800 m. It is immediately clear that the mixed layer did not reach this depth through the duration of the field program, and the ambient LSW layer was probably an older vintage from the Labrador Sea. The high-frequency vertical displacements of the middepth isotherms and isohalines were likely caused by mesoscale fluctuations, which were

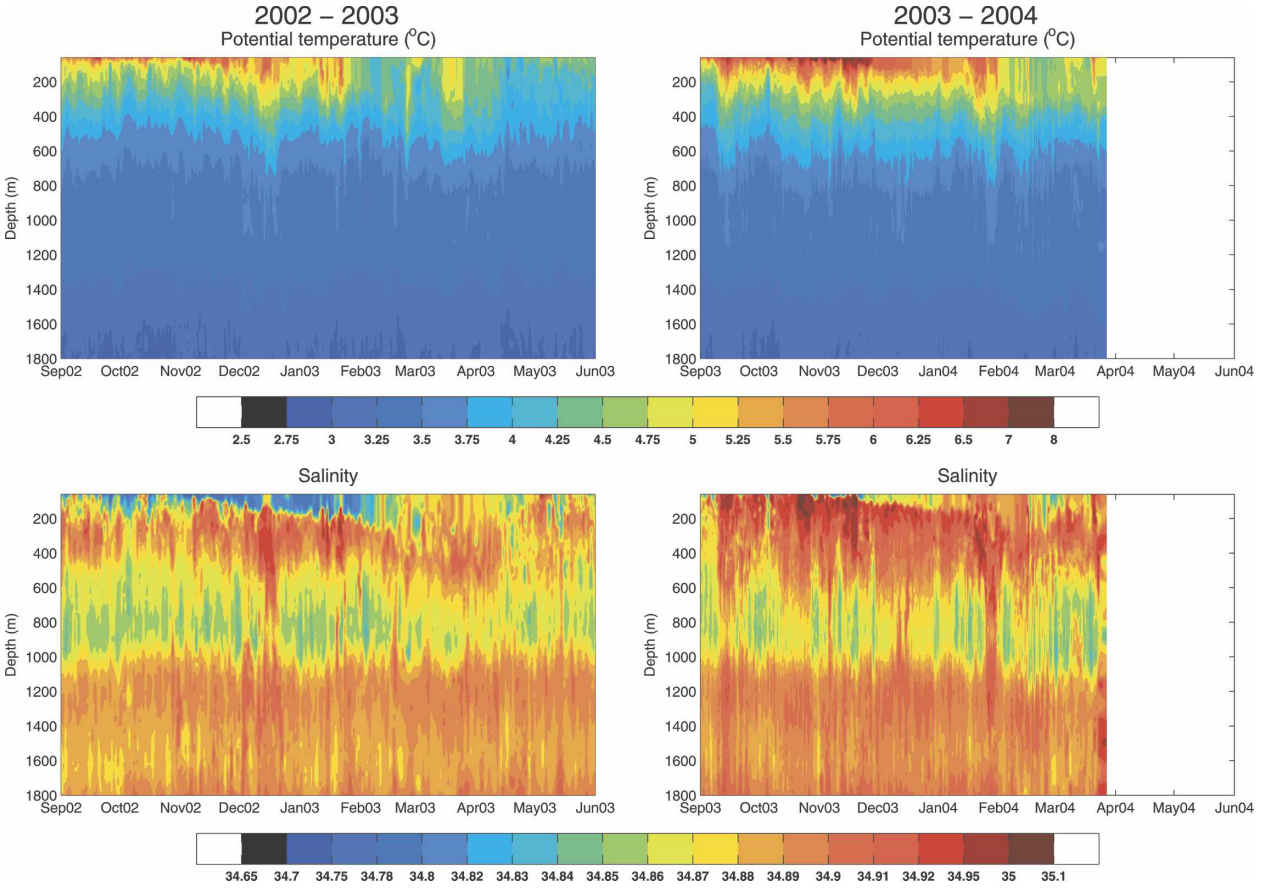

FIG. 3. Time series of potential temperature and salinity from the MP CTD. The left column is for 0203 and the right is for 0304.

generally compensating in density (such variability is not the focus of this study). Surface drifter and satellite altimetry studies show that the interior Irminger Sea is in general a region of relatively low eddy kinetic energy (Fratantoni 2001).

The mixed layer depth for each profile in the MP time series was determined following the procedure of Pickart et al. (2002). To characterize the mean properties of the mixed layer, a linear fit was made to the potential temperature, salinity, and potential density profiles over this depth range. Several of the profiles contained multiple mixed layers, similar to those found by Schott et al. (1996) in the Mediterranean Sea and by Pickart et al. (2002) in the Labrador Sea during active convection. The mixed layer depths for each profile are plotted in Fig. 5 overlaid on buoyancy frequency. For the winter of 0203,[2] mixed layers were first observed below 60 m (the upper limit of the profiler) in the beginning of November. The tendency of the depth of the deepest mixed layers was to increase slowly until the end of January, interrupted by some shoaling events. At the end of January, the mixed layer depth started to increase substantially, exceeding 400 m by the end of the following month, and the buoyancy frequency signature at the base of the mixed layer started to fade as described above. The general depth of the mixed layer was about 400 m until restratification occurred rather abruptly in the middle of April. Mixed layers deeper than 60 m were, however, found until the middle of May.

The mixed layers observed between the middle of February and the middle of April exhibited considerable variability, reaching depths ranging from less than 100 to almost 600 m. Small-scale variability is a phenomenon ubiquitous during the convective process (Schott et al. 1993, 1996; Marshall and Schott 1999). To wit, Pickart et al. (2002) observed significant differences between downcast and upcast traces of shipboard CTD casts during active convection in the Labrador Sea. Even though the convective plumes themselves are

[2] Throughout this work, winter is considered the period from November to April—the period during which mixed layers generally deeper than 60 m were observed.

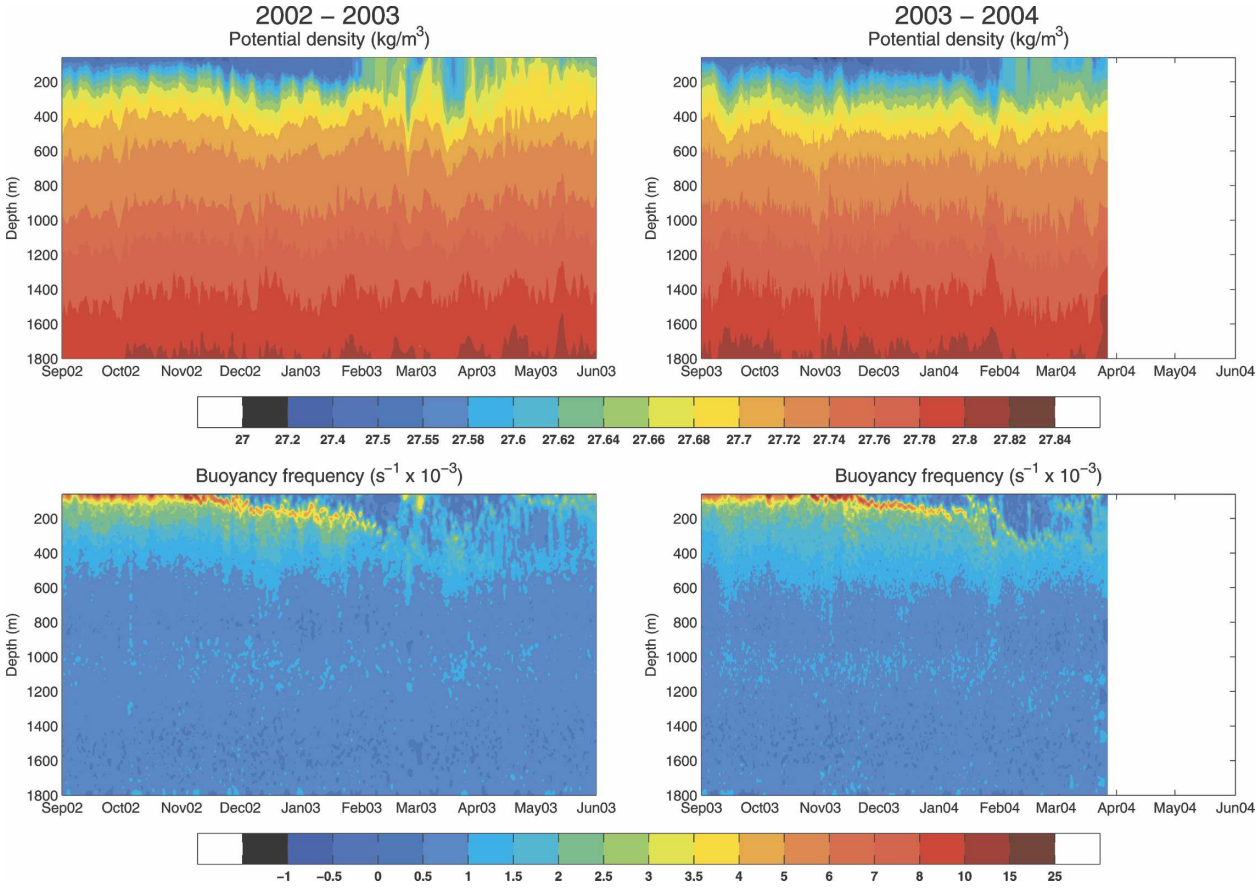

FIG. 4. As in Fig. 3, but for potential density and buoyancy frequency.

localized and intermittent, lateral exchange between the convected water mass and the ambient fluid facilitates spreading along the neutrally buoyant level of the convected water, and the envelope of the mixed layer depths in Fig. 5 is considered the overall depth of convection.

For the winter of 0304, mixed layers were also first observed below 60 m in the beginning of November, and the mixed layer depth developed in a similar way during the first half of the winter (Fig. 5). It did not, however, deepen to the same extent as in the previous winter. The envelope of the mixed layer depth reached about 300 m in the middle of February, and while the individual mixed layers displayed a similar kind of variability, the range was significantly smaller. Mixed layers deeper than 350 m were not observed during the winter of 0304. The MP failed before the final restratification at the end of the winter season occurred. We note that data from profiling floats in the Irminger Sea suggest that the typical thickness of the mixed layer at the end of the winter was about 400 m between 1997 and 2003 (Centurioni and Gould 2004).

4. Air–sea interaction and the effect of the Greenland tip jet

To understand the seasonal evolution of the mixed layer in Fig. 5, as well as the difference in final mixed layer depths between the two winters, the atmospheric conditions during the two winters are now investigated. The major cause of the deepening mixed layer in the southwest Irminger Sea is the passage of winter storms, and, in particular, Greenland tip jet events associated with these storms.

a. Storm tracks

The 6-hourly sea level pressure fields from the NCEP reanalysis were used to track every closed (within 4 mb) low pressure system within the domain shown in Fig. 6. While automated cyclone detection and tracking algorithms are available (e.g., Serreze et al. 1997), the tracking was done by hand because of the high cyclone activity associated with the Icelandic low and cyclone splitting and merging associated with the high topography of Greenland (Petersen et al. 2003; Tsukernik et al.

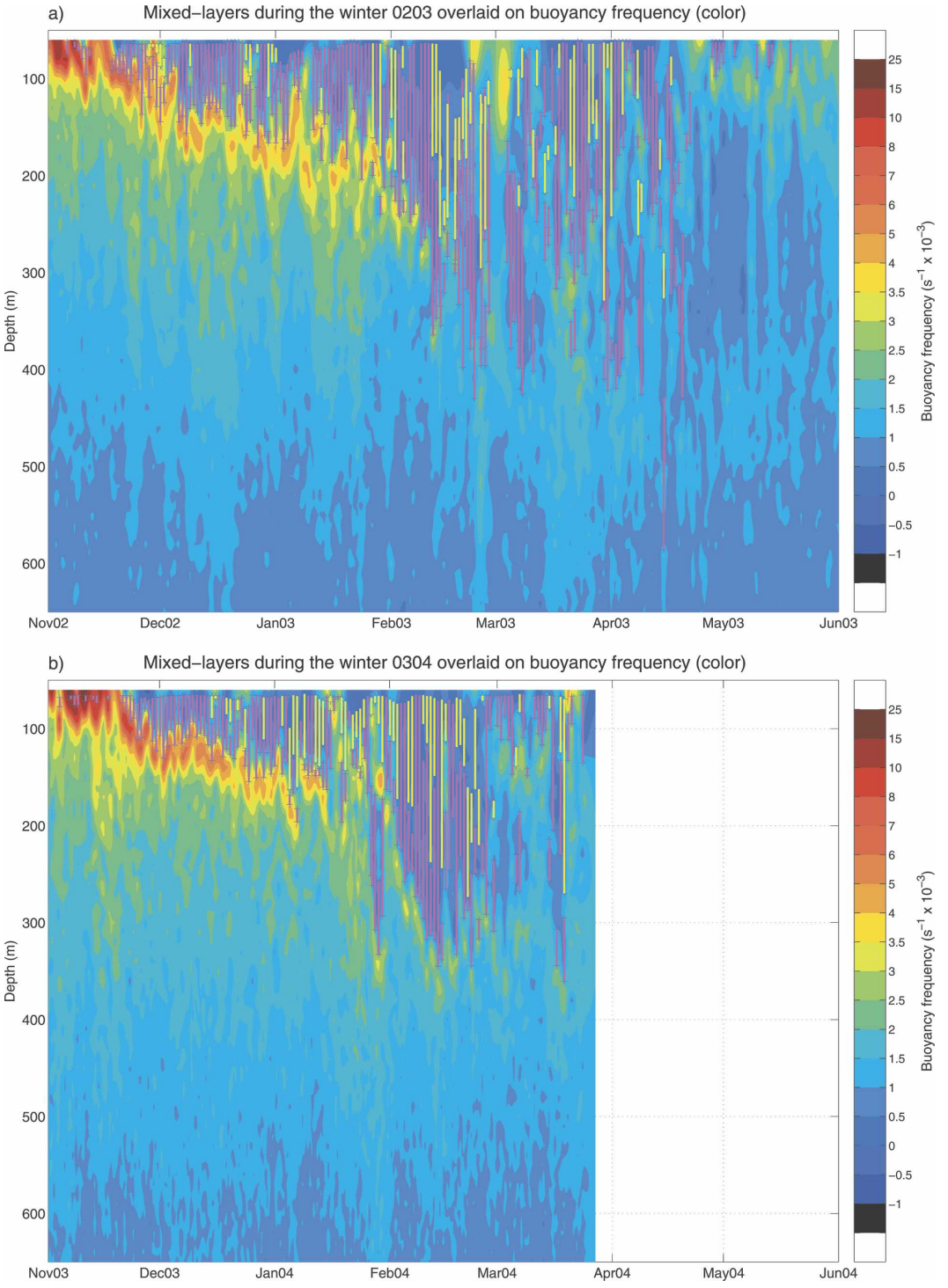

FIG. 5. Time series of mixed layer depth for winter (a) 0203 and (b) 0304. The primary (deepest) mixed layers are indicated by the magenta lines and the secondary (shallower) mixed layers by the yellow lines.

2007). The resulting storm tracks for both winters are plotted in Fig. 6. In general the storms progressed through the domain from southwest to northeast along the North Atlantic storm track (Hoskins and Hodges 2002). During the winters 0203 and 0304, 80 and 96 storms, respectively, were tracked. Several instances of cyclone interaction were observed. Weakening low pressure systems were often overtaken by subsequent

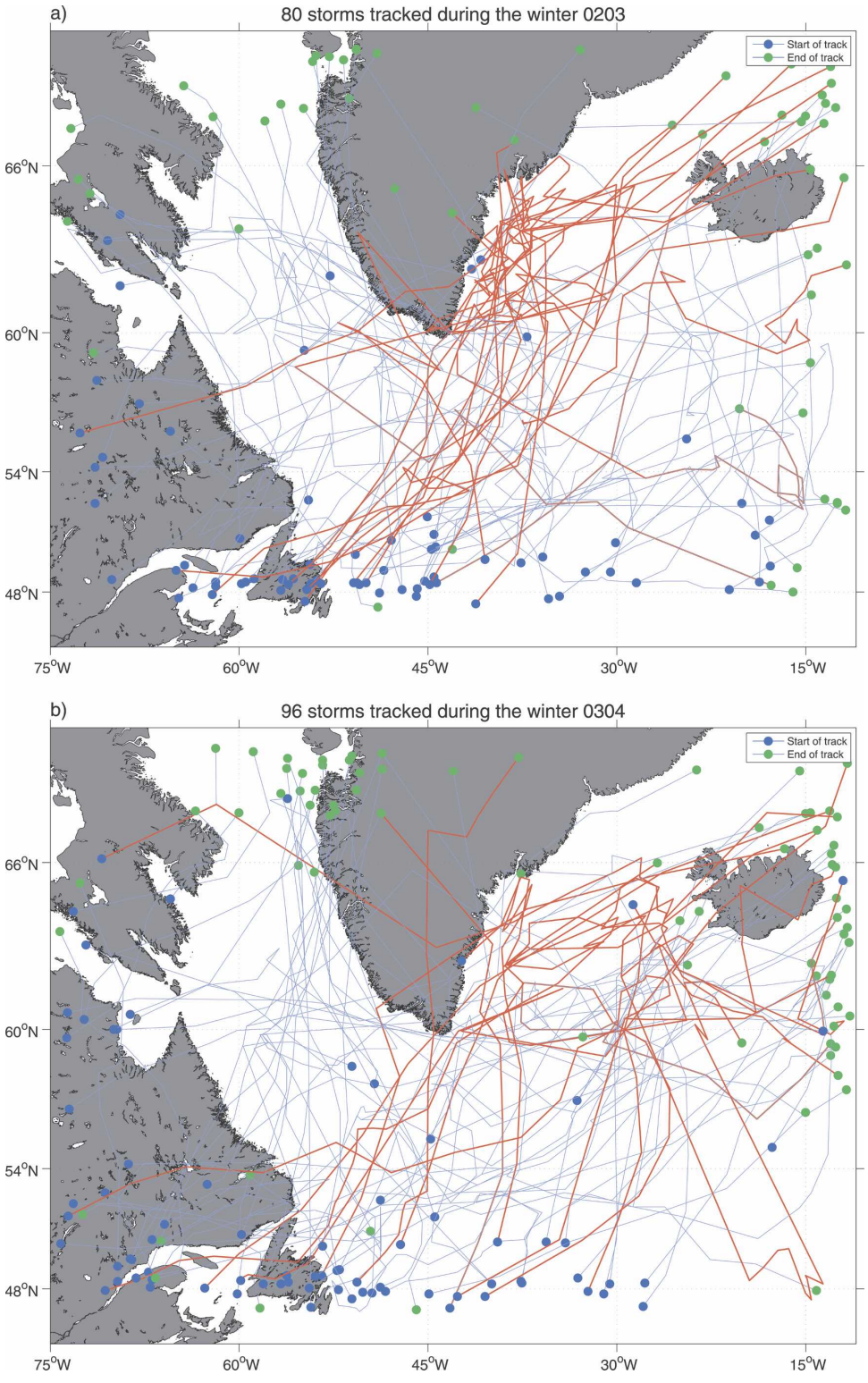

FIG. 6. Closed low pressure systems tracked using NCEP reanalysis data from entry into domain (blue dot) until departure from domain (green dot) for winter (a) 0203 and (b) 0304. Storms directly responsible for causing tip jet events have red tracks.

deeper lows leading to mergers, and there were numerous cases of cyclones splitting south of Cape Farewell and continuing as two separate lows on either side of Greenland.

b. *Signature of tip jet events*

Because of its relatively coarse spatial resolution (1.9°), concerns about the ability of the NCEP wind field to capture small-scale phenomena such as the Greenland tip jet were raised by Pickart et al. (2003b) and Moore (2003). This motivated the use of the higher-resolution (1/4°) QuikSCAT wind dataset. At the latitudes of interest in this study, wind speed and direction data from the SeaWinds scatterometer (Wentz et al. 2001) were available two times daily. Tip jet events were readily recognized by strong zonal (westerly) winds originating near Cape Farewell and extending over the Irminger Sea (see Fig. 2). The NCEP SLP field has a much larger scale than the wind field, and is not significantly affected by the tip jet events. However, the configuration of the SLP gradient field was found to contain a signature of the events.

The same number of tip jet events (17) occurred during each winter, although there was significant variability in their strengths. Figures 7–10 show composites of each winter's tip jet events, with the number of hours given being the time relative to the peak of the event. Each event was associated with a parent cyclone located in the area east of Greenland and north of Cape Farewell, whose position is marked with an L in Fig. 7. For most of the tip jet events, the parent low was situated directly off the southeastern coast of Greenland. Some events, however, occurred when the center of the low was as distant as northeast of Iceland almost 2000 km away. Common for all of the tip jet events, regardless of the position of the parent low, was the pattern of SLP gradients displayed in Fig. 8. Enhanced pressure gradients extending from Cape Farewell over the Irminger Sea were present during all of the events.

Despite some variation in the path of the tip jets, the mean composite wind speed during the peak of the tip jet events exceeded 25 and 20 m s^{-1}southeast of Cape Farewell for the first and second winters, respectively (Fig. 9). The location of the mooring was just north of the region of maximum mean winds, and not all of the individual tip jet events occurred directly above the mooring. Strong northeasterly winds along the eastern coast of Greenland are evident in Fig. 9 as well, particularly for the winter of 0203. These are barrier winds and are also associated with low pressure systems northeast of Cape Farewell (Moore and Renfrew 2005). The mean total turbulent heat fluxes [computed using the bulk formula of Fairall et al. (2003) with QuikSCAT and NCEP surface fields] associated with the tip jet events exceeded the background levels by more than a factor of 4 (Fig. 10). The heat fluxes at the mooring site will be discussed further in section 5a. Despite the low resolution of NCEP, there is a signature of cold air advection due to the tip jets in both the 2-m air temperature and 700–1000-hPa height difference fields (not shown). The composites presented here indicate that the tip jet is a rather short-lived phenomenon, with peak winds generally sustained for less than one day (Fig. 9).

Even though the number of tip jet events and their appearance each winter were similar, there were several important differences. Most notably, the majority of the tip jet events that took place during the winter 0304 were significantly weaker than those of the previous winter, which is reflected in overall higher sea level pressures of the storm centers (Fig. 7), weaker pressure gradients (Fig. 8), lower wind speeds (Fig. 9), and smaller heat fluxes (Fig. 10). A contributing factor to the higher mean tip jet SLP of 0304 was the greater scatter of the parent lows (Fig. 7). The seasonal mean sea level pressure fields for entire winters were also quite different (Fig. 11), even though the NAO index was nearly identical for the two winters. During the winter of 0203, there were both deeper and larger numbers of low pressure systems occupying the area east of southern Greenland. During the winter of 0304, the center of the cyclonic activity associated with the Icelandic Low was shifted eastward, but as the mean sea level pressure near Stykkisholmur, Iceland, did not change much, this shift was not reflected in the NAO index (the winter mean sea level pressures in Lisbon, Portugal, were approximately the same for the two winters according to the World Monthly Surface Station Climatology from the National Climatic Data Center). Such lateral shifts of the center of the Icelandic Low are well known, and latitudinal shifts have recently been related to the frequency of tip jet events (Bakalian et al. 2007).

The tracks of the individual storms that led to tip jet events are plotted in red in Fig. 6. During the winter of 0203, most of the tip jet–producing storms followed a well-defined path that entered the domain near Newfoundland, Canada, proceeded in a northeastward direction past Cape Farewell through the Denmark Strait, and left the domain northeast of Iceland. By contrast, the storms that caused tip jets during the second winter followed no such "highway." Instead the tracks were distributed throughout most of the western North Atlantic. The main reason for this difference is the steering currents, which are the prevailing upper-level flow patterns that govern the movement of

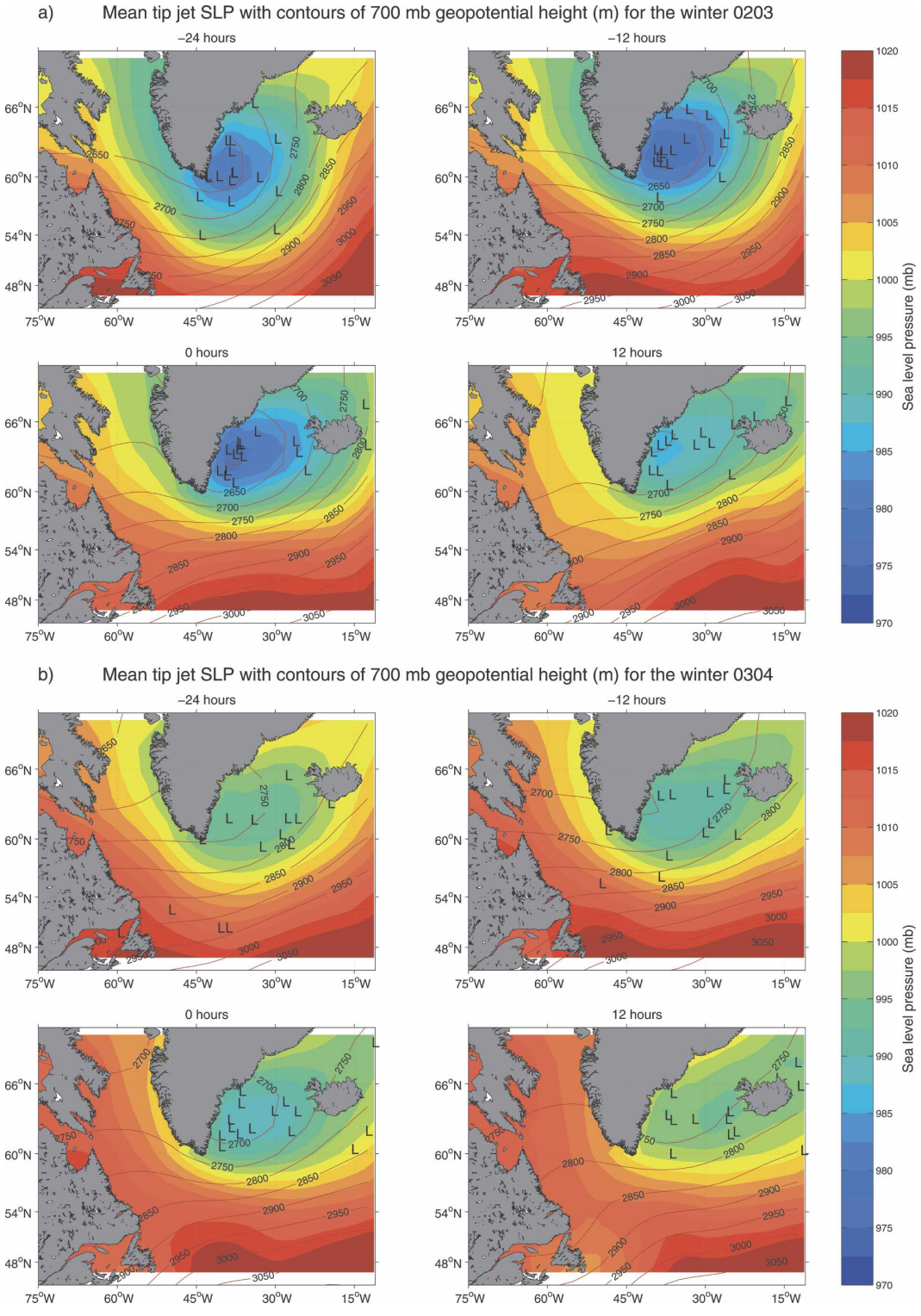

FIG. 7. Composite of NCEP SLP (color, mb) during all of the tip jet events for winter (a) 0203 and (b) 0304. Overlaid on this is the height of the 700-mb geopotential surface (contours, m), which is a measure of the upper-level steering currents. The given times indicate hours before and after the peak of the tip jet event, and the L marks the center of the parent low pressure system.

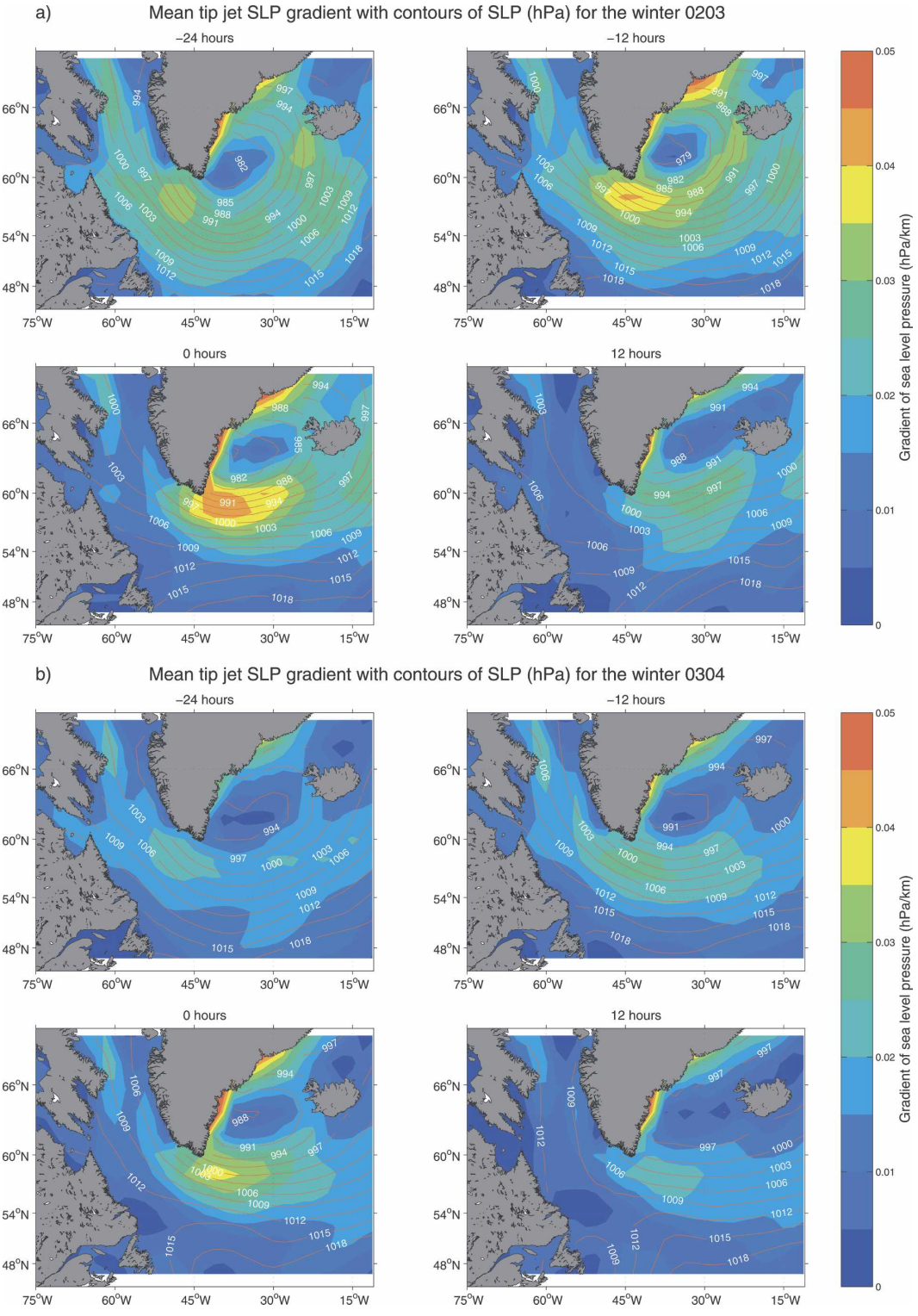

FIG. 8. Composite of NCEP SLP gradient (color, mb km^{-1}) during all of the tip jet events for winter (a) 0203 and (b) 0304 with contours of SLP (mb) overlaid.

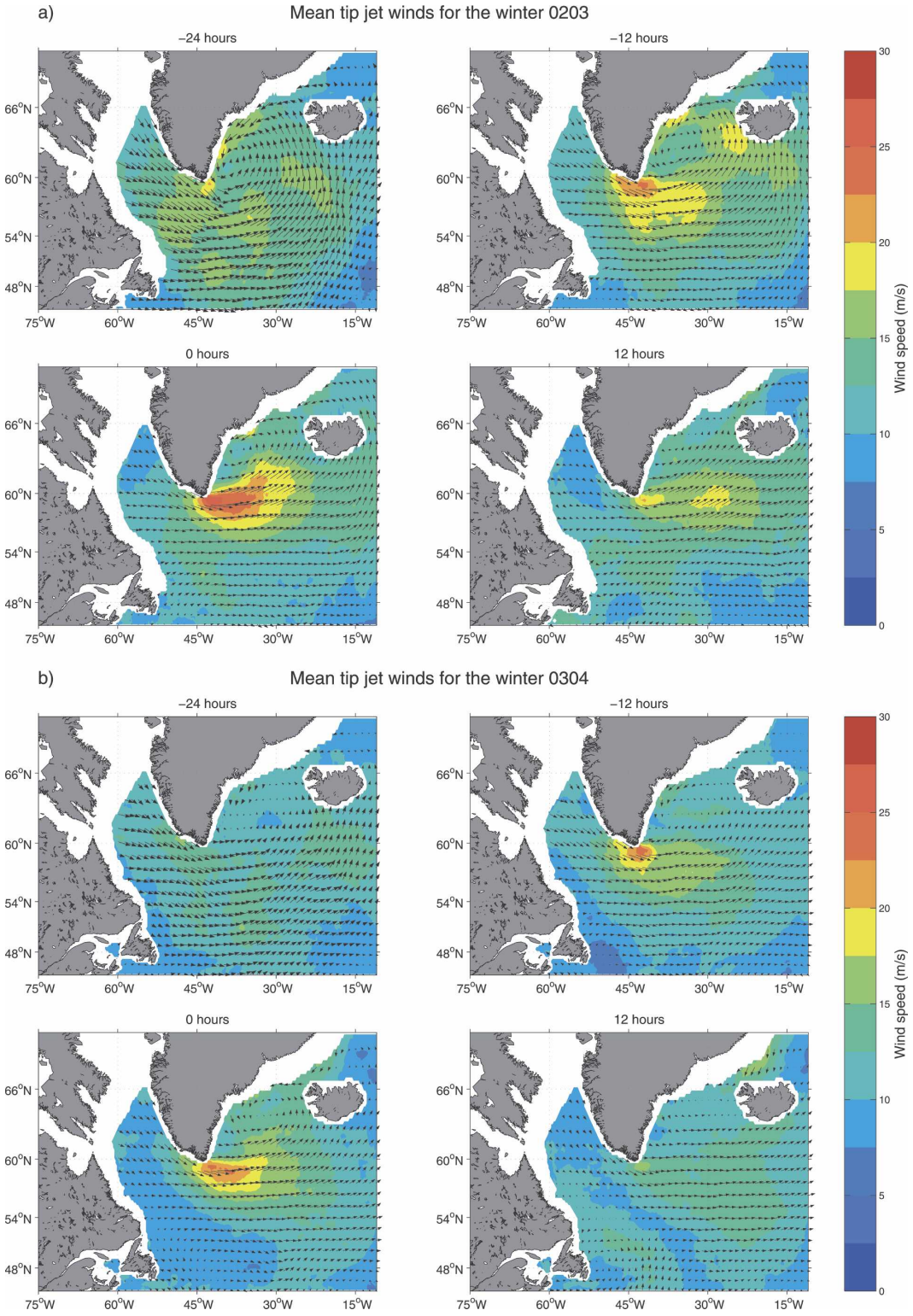

FIG. 9. Composite of QuikSCAT 10-m wind speed (color, m s^{-1}) during all of the tip jet events for winter (a) 0203 and (b) 0304. Every 25th wind vector is plotted, and only grid points with more than 5 realizations are included in the average.

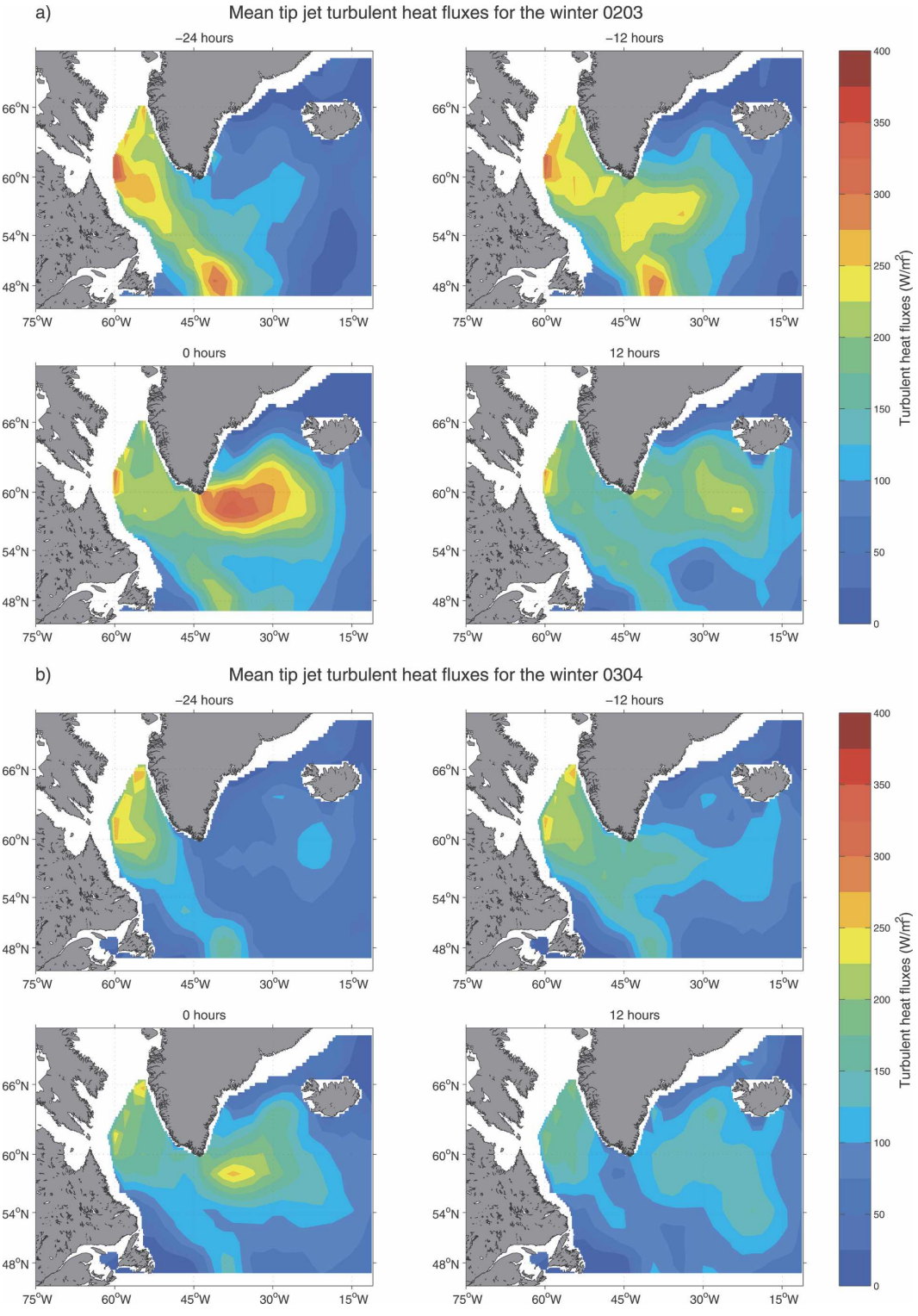

FIG. 10. Composite of total turbulent heat fluxes (color, W m^{-2}) during all of the tip jet events for winter (a) 0203 and (b) 0304.

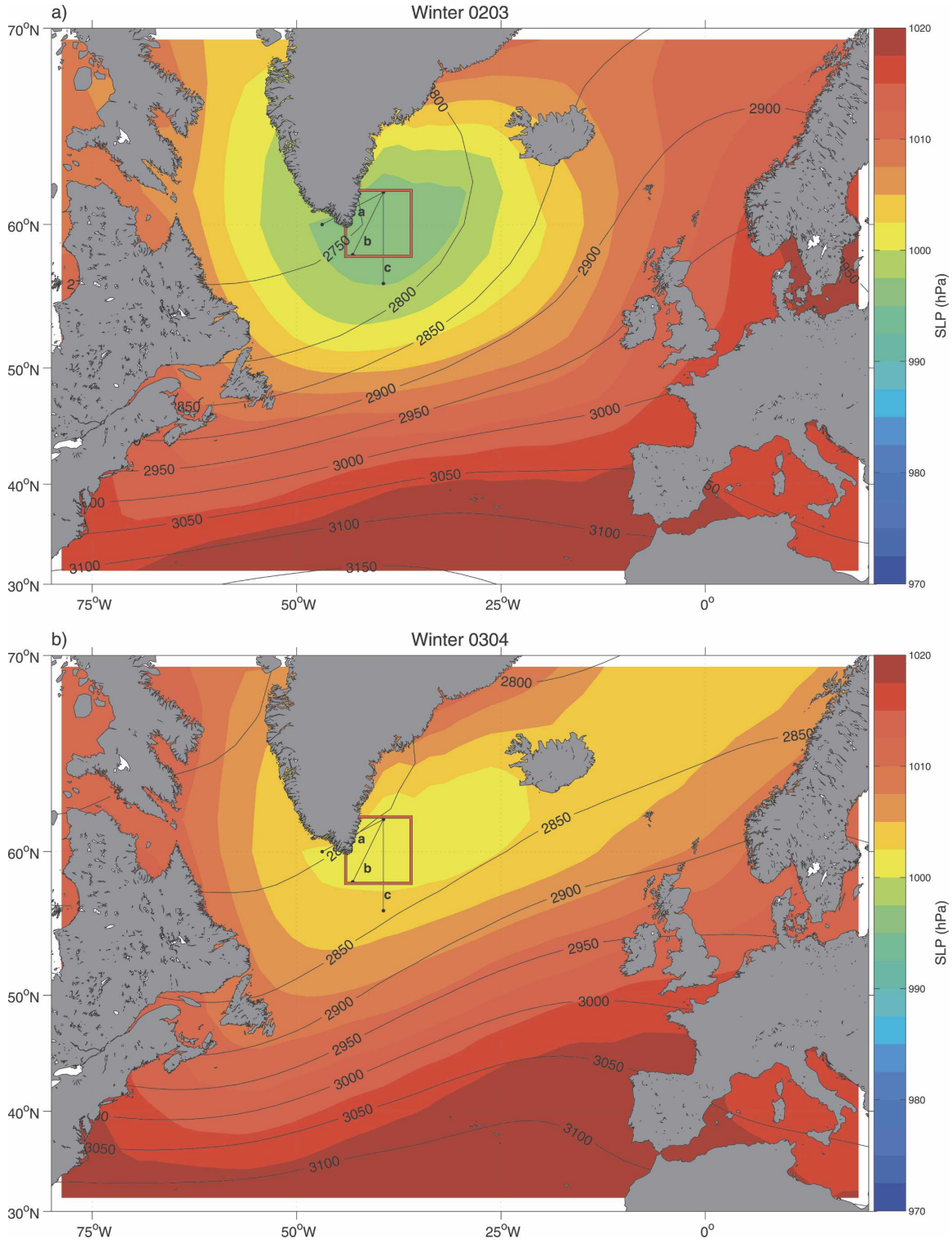

FIG. 11. Mean NCEP SLP (color, mb) and 700-mb geopotential height (contours, m) for winter (a) 0203 and (b) 0304. See text for explanation of the box and the lines.

smaller embedded low-level features. Figure 11 shows the mean 700-mb geopotential height patterns for the two winters. Note that the contours were oriented in a more meridional direction near Cape Farewell during the first winter, causing more lows to enter the Irminger Sea and become situated in the lee of Greenland (as in Fig. 7 at 0 h). By contrast, the more zonally oriented contours of the second winter tended to advect the low pressure systems across the North Atlantic without focusing them near Greenland, which apparently is unfavorable for the generation of strong tip jets. On a larger scale, the winter of 0203 may be classified according to Vautard (1990) as being associated with a "blocking" regime, while the conditions for the winter of 0304 were more similar to the "Atlantic ridge" regime. Although these regimes may not last for more than a couple of weeks at a time, they appear to be the dominant modes that occurred during these two winters.

Some storms were advected through the area east of Greenland without leading to tip jet events (Fig. 6). We believe that these storms failed to produce tip jets because they did not result in the pressure gradient field associated with the canonical tip jet event (Fig. 8), either because of interaction with another low pressure system or because the pressure associated with the cyclone was not low enough relative to the ambient sea level pressure south and west of Cape Farewell.

c. *Objective detection of tip jets*

Using data from the Prins Christian Sund meteorological station (labeled PCS in Fig. 1), Pickart et al. (2003b) determined that tip jet events were characterized by strong westerly winds, anomalously low air temperatures, and low sea level pressure. They used empirical orthogonal functions (EOFs) with the PCS data to identify objectively the occurrence of tip jet events over a period of approximately 30 yr. The storm tracks (Fig. 6) and the composite images (Figs. 7–10) indicate that the occurrence of a tip jet event is dependent on more than a storm's central pressure, and suggest that the gradient of SLP might be a better metric. As described above, intensified pressure gradients from Cape Farewell over the Irminger Sea were observed during each tip jet event, regardless of the position and strength of the parent cyclone. The varying path of the tip jet and the suspected influence of the high local topography make the zonal winds from the PCS meteorological station, as used by Pickart et al. (2003b), less than ideal.

A new EOF approach has therefore been devised in which zonal winds, pressure gradients, and air temperature were employed. For the wind time series, QuikSCAT data were used. In particular, at each point in time the maximum zonal wind within the red box of Fig. 11 was determined, thereby taking into account the shifting path of the tip jets. Although the temporal resolution of QuikSCAT is lower than PCS (12 versus 3 h), the QuikSCAT winds at the mooring site are not influenced by fjord effects as the coastal met station data may be. Pressure gradients were computed along the lines labeled a, b, and c in Fig. 11 using the NCEP sea level pressure field, and the mean of these three values was used. Although a temperature signal was evident in the NCEP reanalysis, its coarse resolution makes it unsuitable to capture accurately the small-scale signature of the Greenland tip jet.[3] Ideally, an equivalent roving air temperature time series, tied to the position of the maximum QuikSCAT zonal wind, should be used. Unfortunately, no product with the desired resolution and accuracy is presently available, and the PCS temperature data were deemed the best available choice. This introduces the possibility of tip jets evading the meteorological station and thus leaving no temperature signature. Inspection of the zonal wind and temperature PCS time series at the times of the observed tip jet events implied that two of the observed tip jet events in the first winter and four in the second were undetectable at the meteorological station. These were, however, among the weakest events that occurred, and the signatures of all of the more robust events were clearly detectable in the PCS data.

The EOF calculation was done for the months of November through April, and the dominant mode of variability for both years was that due to tip jet occurrences. The strength of the events varied throughout the winter, and those in which the reconstructed zonal wind speed exceeded 25 m s^{-1} were designated as robust tip jet events. In the winter of 0203, 16 of the 17 events passed this criterion and accounted for 65% of the variance in the time series. The winter 0304 contained overall weaker tip jet events; only 11 of the 17 tip jets that occurred were robust, and 58% of the variance was explained. As a check on the EOF calculation, the data were inspected manually for the signature of tip jet events, and no robust events were found that were not detected by the EOF approach. Conversely no tip jet events were detected by the EOF that escaped manual detection. All of the events that did not pass the 25 m s^{-1} criterion had either below-average zonal winds or distorted pressure gradients preventing the formation of robust tip jets. Comparison of the EOF method employed here with the method of Pickart et al. (2003b)

[3] The NCEP SLP gradient field has a much larger tip jet signature.

indicates that the new method is more sensitive. Using data from the PCS meteorological station alone [as Pickart et al. (2003b) did], only 6 robust tip jets were identified and 52% of the variance was explained for the winter of 0203, and 7 strong events were detected and 45% of the variance was explained for the winter of 0304. This indicates that the meteorological weather station data are influenced by other phenomena, such as fjord effects, and that the EOF approach devised here is better suited for identifying tip jet occurrences.

To determine the number of tip jet events directly affecting the mooring site, the QuikSCAT wind at this location, obtained through spatial interpolation, was used in the EOF computation instead of the wind at the roving point. The pressure gradient and temperature time series remained unchanged, while the reconstructed zonal wind speed criterion for designation as a robust tip jet event was lowered to 20 m s^{-1}. The resulting number of robust tip jet events at the mooring site was 12 and 5 for the winters of 0203 and 0304, respectively. Meridional variation in the path of the tip jets was the reason for the reduced number of strong tip jet events. The occurrences of the strong events impacting the mooring site and the development of the depth of the deepest mixed layer are plotted in Fig. 12. This figure suggests that the discrepancy in the mixed layer depths for the two years may be largely attributable to the differences between the two winters' tip jet events. The considerable deepening of the mixed layer in February 2003 happened during a concentrated set of tip jet events (7) that occurred just before and during that month. By contrast, the five robust storms that directly affected the mooring site during the winter of 0304 were more scattered in time (and two of them occurred after the moored profiler failed). The integrated effect of the heat loss through the winter governs deep convection, which is more likely to occur when concentrated in intense storms rather than distributed evenly but more weakly throughout the winter (Marshall and Schott 1999). It is shown below that the heat fluxes resulting from tip jet events do indeed have a significant impact on the depth of the mixed layer in the southwest Irminger Sea.

5. Heat fluxes and 1D mixed layer deepening

a. Best-estimate fluxes

The concerns raised about NCEP's ability to capture accurately the Greenland tip jet (Pickart et al. 2003b; Moore 2003) seem to be warranted. For instance, during the tip jet events of 0203 the zonal winds as measured by QuikSCAT were almost twice as strong as those found in NCEP. Furthermore, Renfrew et al. (2002) found that neither the NCEP humidity nor the sea surface temperature fields agreed particularly well with in situ wintertime observations in the Labrador Sea, and both air temperature and humidity are expected to be strongly influenced by tip jet events. For these reasons, we have developed new turbulent heat flux time series for the mooring site in the Irminger Sea using bulk formulas.

Time series of wind, humidity, and air and sea surface temperatures are required for the computation of the turbulent heat fluxes. Wind data were obtained from a spatial interpolation of the QuikSCAT scatterometer data to the mooring site, and sea surface temperature was obtained from an extrapolation to the surface of the MP mixed layer values using the linear fit described in section 3. For both winters, the root-mean-square (rms) differences between the extrapolated SST and satellite SST observations (which are sparse because of cloud cover) were 0.5°C and the extrapolated SST was on average 0.1°C warmer than the satellite SST. For air temperature and humidity, our best choices were the PCS weather data and NCEP fields, respectively. Fortunately, a meteorological buoy deployed at the mooring site from August to December 2004 provided valuable time series for calibration of both these quantities. In particular, scaling factors were determined for both variables to make them applicable to the mooring location. Such a scaling was justified since the respective buoy time series were significantly correlated with the PCS air temperature, NCEP humidity, and QuikSCAT wind time series. Details of the adjustment procedure are found in Våge (2006). Finally, the bulk formula of Fairall et al. (2003) was used on the time series to produce turbulent heat fluxes at the mooring site. Hereafter we refer to these as the "best-estimate" fluxes, while the NCEP heat fluxes considered for comparison are the flux-corrected product of Renfrew et al. (2002).

The comparison between the best-estimate total turbulent (latent plus sensible) heat fluxes and those from NCEP is shown in Fig. 13. The best-estimate mean winter heat fluxes were larger by 33% in 0203 (100 versus 75 W m^{-2}) and 40% in 0304 (95 versus 68 W m^{-2}) when computed by the Fairall et al. (2003) bulk formula. Without exception, all of the high heat flux events in 0203 and 0304 (those exceeding 400 W m^{-2}) occurred during tip jet events. During a high-NAO winter, a greater number of large heat flux events would be expected, and the heat loss concentrated in those storms can be very effective in driving deep convection (Marshall and Schott 1999). The radiative heat flux terms have smaller magnitudes and are to a much lesser ex-

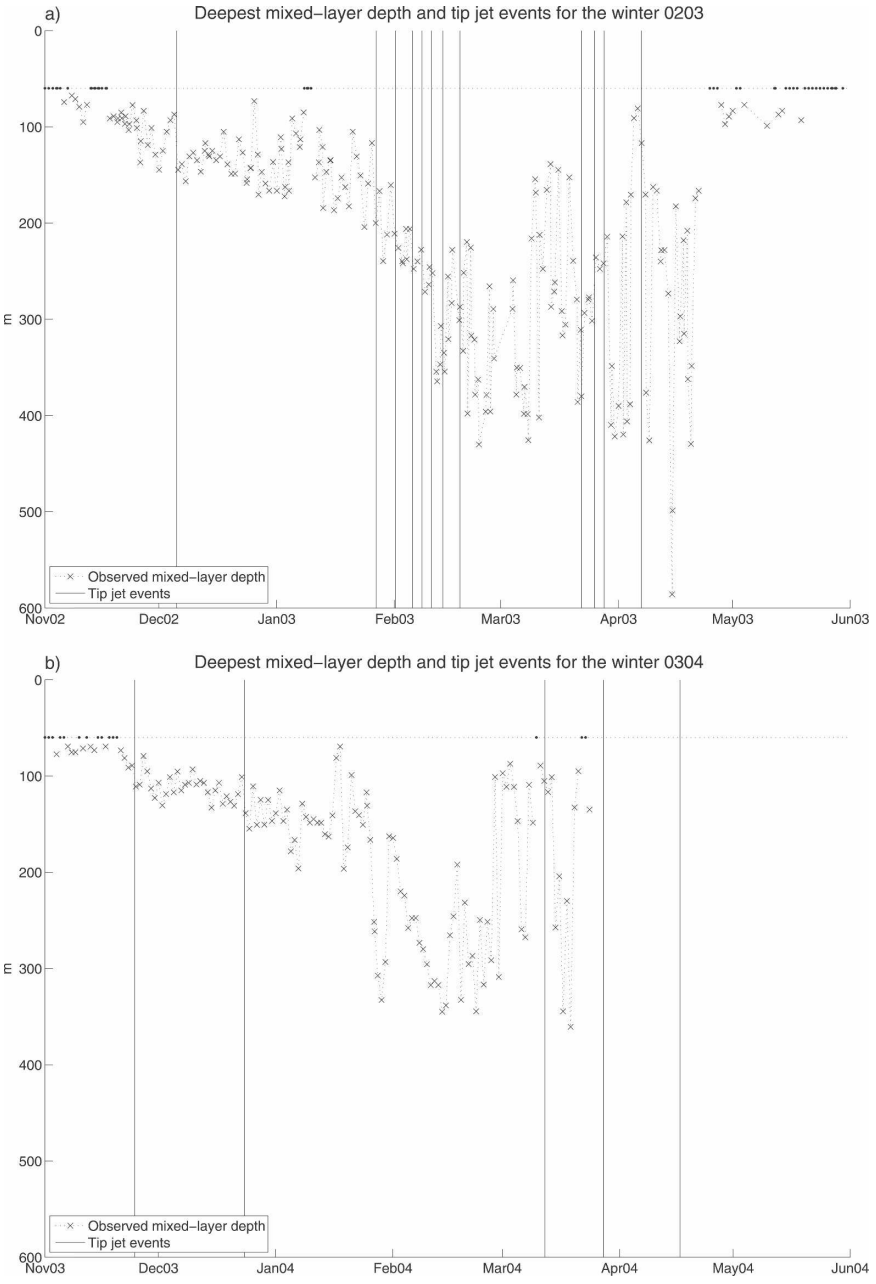

FIG. 12. Depth of the deepest mixed layer (black *x*'s) for winter (a) 0203 and (b) 0304. The heavy black dots identify profiles for which no mixed layer was observed below 60 m. Robust tip jet events are indicated by the vertical lines.

tent influenced by the tip jet events, and the NCEP radiative flux fields were used as is. It should be noted that the freshwater flux can also be significant for the development of the mixed layer, but, as for the Labrador Sea, the buoyancy contribution of the evaporation–precipitation difference for the Irminger Sea is small compared with the heat fluxes (Marshall and Schott 1999).

b. Mixed layer model

To shed light on the cause of the wintertime mixed layer development in the Irminger Sea as observed by the MP mooring, a one-dimensional mixed layer model (Price et al. 1986, hereafter PWP) was employed. Within the Irminger Sea gyre the mean currents are relatively weak—on the order of 2–3 cm s^{-1} from our

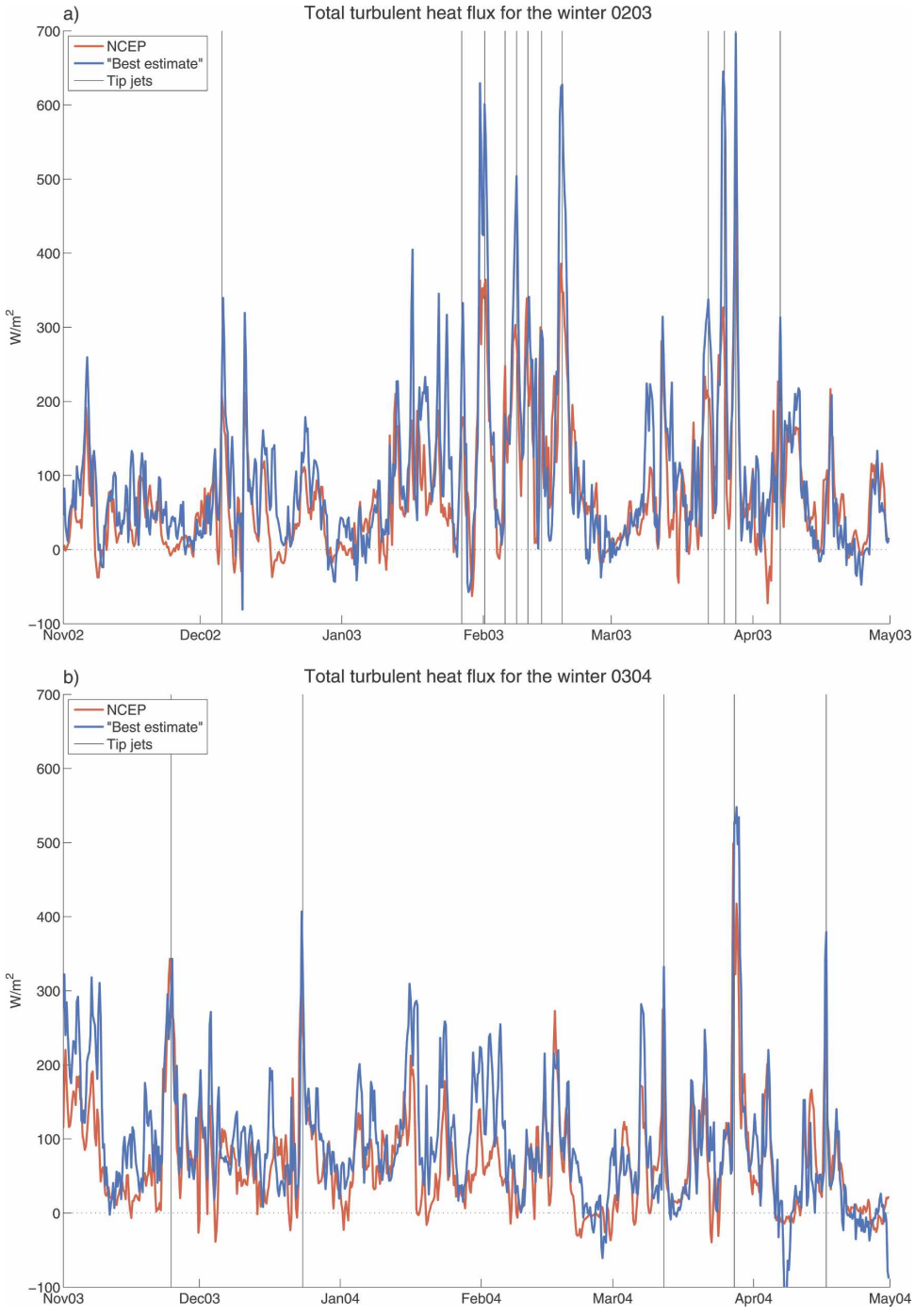

FIG. 13. Comparison of NCEP (red) latent plus sensible heat fluxes at the mooring site with those computed in this study using the bulk formula of Fairall et al. (2003) (blue) during winter (a) 0203 and (b) 0304. Positive heat fluxes are directed out of the ocean. The occurrences of robust tip jet events are marked by the vertical black lines.

ACM data and from Lavender et al. (2005)—and it is an area of relatively low eddy kinetic energy (Fratantoni 2001). The cyclonic circulation traps the water within the gyre, and a 1D mixed layer model predicted with skill the evolution of the mixed layer under similar conditions in the Labrador Sea (Bramson 1997). For these reasons, a 1D approach is assumed reasonable to first order in this setting. We emphasize that the aim

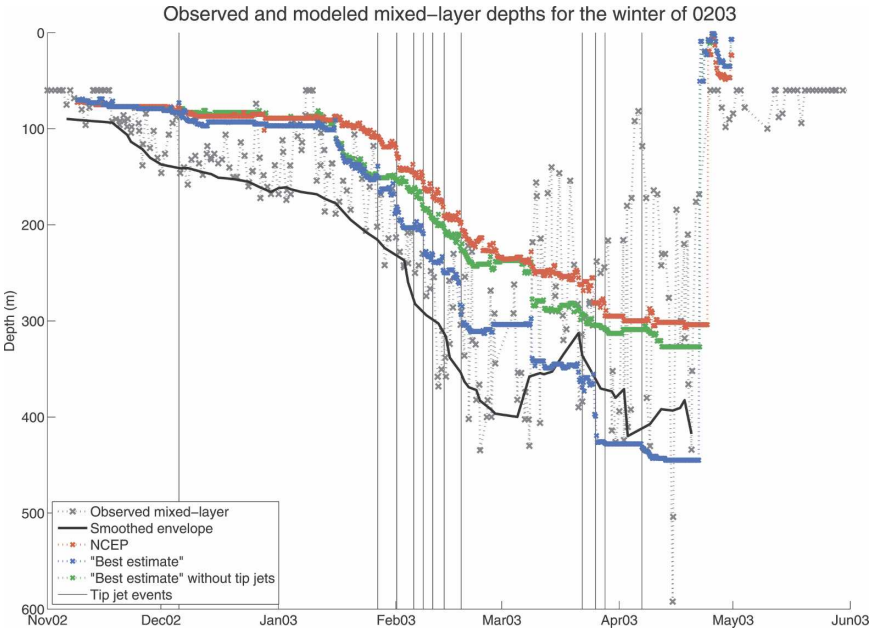

FIG. 14. Comparison of observed mixed layer depth and modeled mixed layer depth for winter 0203 using the 1D PWP model. The separate model runs were forced with NCEP surface fluxes (red), the best-estimate fluxes described in the text (blue), and the best-estimate fluxes with the tip jet events removed (green). The thick black curve is the low-passed envelope of the observed mixed layer depths (see text).

here is not to reproduce the detailed structure of the mixed layer depth time series, which is impossible without taking advection into account, but to understand better the overall evolution of the wintertime mixed layer expressed by the envelope of the deepening, and in particular the effect that the tip jet events have on this.

To implement the PWP model, the fluxes of heat, freshwater, and momentum were imposed at the surface at each time step, and mixing was carried out until three different stability criteria were satisfied. These involved the vertical density gradient (static stability), the bulk Richardson number (mixed layer stability), and the gradient Richardson number (shear flow stability). The latter two conditions describe wind mixing processes, as the velocity appearing in the Richardson numbers is entirely wind driven, and both processes would be inactive without wind. The vertical grid extended from the surface to 1000 m, with 2-m resolution.

We forced the model with our best-estimate heat fluxes and, for comparison, with the NCEP heat fluxes. We used a time step of 6 h, which is marginal in terms of resolving the inertial period (about 14 h at the latitude of the mooring). However, comparison of model results using PCS wind stress with a time step of 3 h and subsampled PCS winds with a time step of 6 h showed no significant difference in terms of mixed layer depth, which indicates that resolution of the inertial period is not critical to this study. Furthermore, sensitivity studies indicate that the direct effect of wind stress is secondary compared with the effect of the total turbulent heat flux, and also confirm that the effect of the freshwater flux is very small (Våge 2006).

1) WINTER 0203

Figure 14 shows a comparison of the observed and modeled mixed layers for the winter of 0203. The model was initialized with the low-pass-filtered average MP profile for the first half of November 2002, and each run started on 8 November and lasted until the end of April. The model mixed layer depths were determined automatically using the method of Lorbacher et al. (2006), which identifies the shallowest extremum of curvature of the potential density profile with the base of the mixed layer. For less than 4% of the profiles, a shallow mixed layer was found instead of the deeper primary mixed layer. These appeared as spikes in the mixed layer depth time series, and were interpolated over. Since the model does not include advection, it is more meaningful to compare it to the envelope of the deepest observed mixed layers. The envelope was computed by considering every local maximum of the mixed layer depth time series and smoothing the result using a running mean filter.

For the first run, the model was forced with NCEP surface fluxes only, and the depths of the deepest mixed layers are indicated by the red curve in Fig. 14. The second run was forced with the best-estimate heat fluxes computed with the bulk formula of Fairall et al. (2003) and with momentum fluxes (wind stress) computed from the QuikSCAT dataset, and the result is plotted in blue. To assess the importance of tip jet events on convection, a third run was carried out in which the tip jet signature was removed (via interpolation) from the best-estimate heat fluxes and QuikSCAT momentum fluxes. With the tip jet events removed, the mean total best-estimate heat flux over the entire winter was reduced by 27% to 79 W m^{-2}. The modeled mixed layer depths for the no tip jet case are indicated by the green curve in Fig. 14.

The NCEP as well as the best-estimate heat fluxes produce time series of model mixed layer depths that display the general character of the observed envelope of deepest mixed layer depths, with gentle deepening early in the winter, a more rapid deepening during late January and February, and restratification in late April. However, Fig. 14 indicates that the NCEP heat fluxes are too weak to produce the extent of mixed layer deepening observed by the MP. By contrast, the mixed layer resulting from the best-estimate heat fluxes is ~150 m deeper and follows the envelope of the observations more closely, reaching a maximum depth in excess of 440 m. Because of NCEP's inability to properly resolve tip jet events, one would expect that this discrepancy is at least partly due to the enhanced heat loss caused by the high wind speed tip jet events. The final model run in Fig. 14 shows that this is indeed the case and that the tip jets had a significant effect on the evolution of the mixed layer in the winter of 0203. The difference between the model results with and without tip jets became particularly large during the periods of frequent tip jet events in early February and late March. Hence, the integrated effect of the intense heat fluxes associated with the tip jet events, in particular when several tip jets occur in short succession, plays an important role in the development of the mixed layer in the Irminger Sea.

Although the general envelope of mixed layer depth is fairly well captured by the PWP model forced by the best-estimate fluxes, there are significant discrepancies between the model and the observations, especially regarding the high-frequency variability that is not captured by the model (Fig. 14). This is likely due in part to the missing effect of lateral advection. The mixed layers predicted by the PWP model can only be changed by surface fluxes. In the real ocean, this is not the case. Small-scale variability is ubiquitous during active convection (Pickart et al. 2002), and the effects of advection and mesoscale events distort the mixed layer, which is evident by the range of mixed layer depths observed during the second half of each winter in our records. However, as the site of the mooring was located within the Irminger Sea gyre, in an integrated sense approximately the same body of water was subjected to the heat removal indicated by the best-estimate heat fluxes throughout the winter, and the final depth of the mixed layer is assumed to be closely related to the total amount of heat removed from the surface of the gyre. In this regard, the envelope of the MP mixed layer depths is considered a more appropriate quantity to be directly compared with the model results.

2) WINTER 0304

Figure 15 compares the observed and modeled mixed layers for the winter of 0304. As before, the initial profile was the low-pass-filtered average MP profile from the first half of November, and the model was run from 8 November to the end of April with the same three sets of surface fluxes as in the previous winter. Again it was found that the NCEP heat fluxes resulted in too shallow mixed layers, while the best-estimate heat fluxes generated model mixed layer depth time series that reached 100 m deeper, in better agreement with the observations. Because of the low number of robust tip jet events during this winter, the difference between the results produced by the best-estimate heat fluxes with and without tip jets was minor. Since the MP failed before restratification occurred, comparison of the observations and model regarding the timing of the restratification for the second winter was not possible.

Considering both the data and the model results, the depth of convection during the second winter was approximately 100 m shallower than for the first winter. In addition to the atmospheric conditions, the initial stratification of the ocean plays an important role in determining the final depth of the mixed layer (e.g., Lazier et al. 2002). At the start of the winter 0203, the water column at the mooring site was better preconditioned (i.e., more weakly stratified than at the start of the winter 0304) and thus weaker surface fluxes were required to deepen the mixed layer to an equivalent depth for the first winter compared with the second. However, the difference in initial stratification between the two winters under consideration was not very significant. When the NCEP heat fluxes from the winter of 0304 were used to force the PWP model with the November 0203 initial profile, the mixed layer reached only 10 m deeper than when the November 0304 initial profile was used. This further supports the conclusion

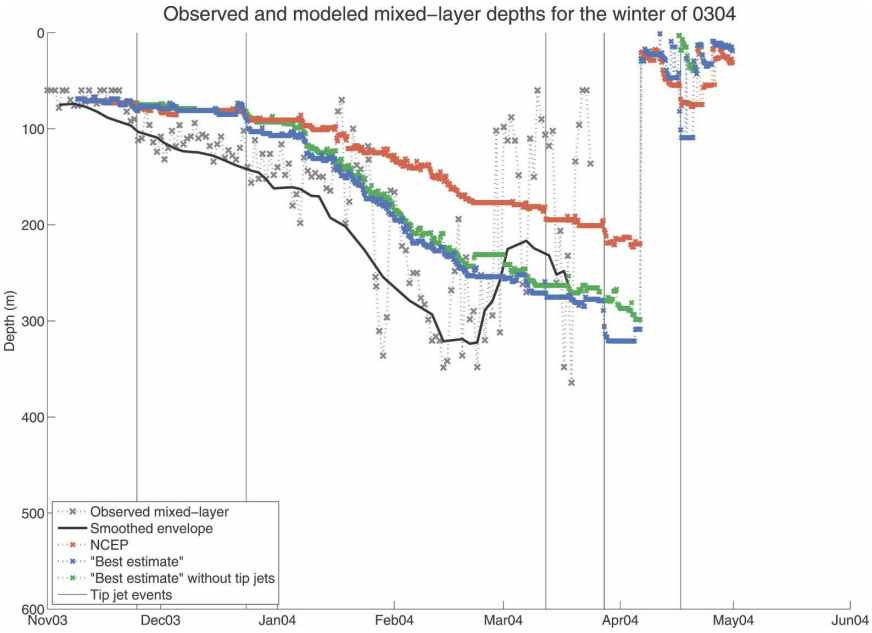

FIG. 15. As in Fig. 14, but for winter 0304.

that the greater number of tip jets in the first winter was a key reason for the deeper convection.

3) WINTER 9495

The good agreement between the observed envelope of convection and the modeled mixed layer depths over the two winters when forced by the best-estimate heat fluxes encouraged application of the model to a more robust winter, particularly one during the high-NAO period of the early 1990s when convection reached great depth in the Labrador Sea. The idea is that convection might have reached similar depths in the Irminger Sea because of repeated robust tip jet events. Unfortunately, there were no mooring time series for verification of the results, but the World Ocean Circulation Experiment (WOCE) A1E CTD line passes over the mooring site and there were quasi-annual occupations of the line during this period. One of the A1E CTD stations near the mooring site taken in late November 1994 provided an initial profile for the model, and the model grid was extended to 2000 m with the same vertical resolution. The winter 9495 was near the end of the high-NAO period of the early 1990s, and presented a well-preconditioned ocean and above-average heat fluxes.

As scatterometer data were not yet available for the winter of 9495, we constructed a heat flux time series using an alternative approach. Specifically, the PCS zonal winds were used, after adjustment of the time series to the mooring site based on comparison to the QuikSCAT zonal winds during the years of mutual overlap. The NCEP meridional winds were used since the PCS weather station is located adjacent to a zonally oriented sound (keep in mind that the meridional winds are of secondary importance for the heat flux). Finally, the NCEP SST data were used after scaling the time series via comparison to the extrapolated MP SST for the winters of 0203 and 0304. As a check on this overall approach, an analogous heat flux time series for the winter of 0203 was constructed, which compares favorably to the best-estimate time series computed above for that winter. When this alternative 0203 heat flux time series is used with the PWP model, the final mixed layer depth differs by less than 10 m from the best-estimate case in Fig. 14. This gives us confidence that the procedure used to compute the 9495 heat fluxes is sound.

The mean total heat flux constructed as such for winter 9495 was 125 W m^{-2}, 35% greater than the original NCEP heat flux. This percent increase is comparable to that of the best-estimate heat fluxes for winters 0203 and 0304 relative to the NCEP heat fluxes. The occurrences of the tip jet events for this winter were determined using the EOF approach of Pickart et al. (2003b), indicating that there were 13 robust events.[4] At the end of the convective season, the mixed layer depth for the model run forced with the best-estimate

[4] Based on the results of section 4c, this is likely an underestimate.

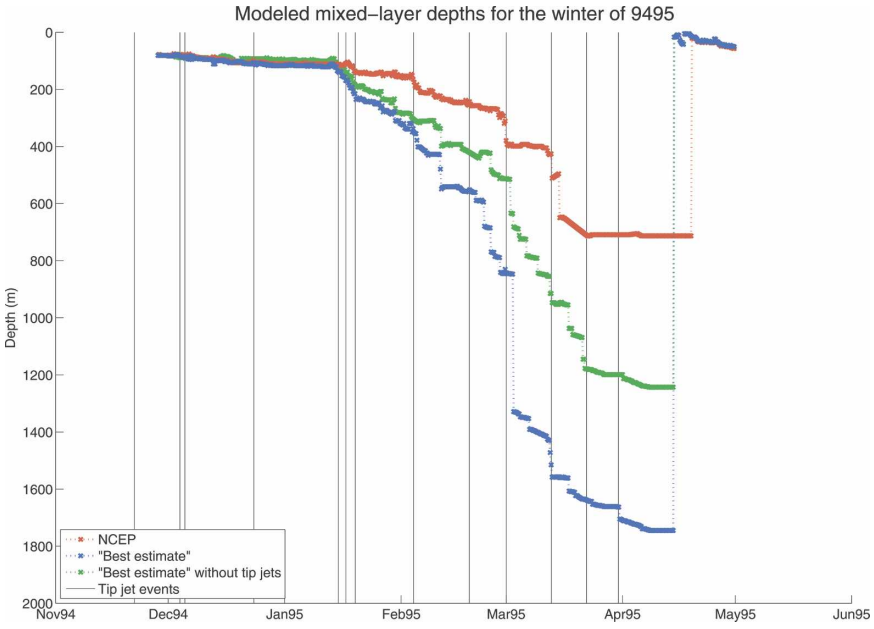

FIG. 16. As in Fig. 14, but for winter 9495.

fluxes reached a depth of about 1750 m (Fig. 16). This is consistent with the summer 1995 WOCE A1E CTD data indicating that convection reached 1700 m that winter (Pickart et al. 2003a). This is slightly less than the convective depth observed in the Labrador Sea during the same winter (Lilly et al. 1999). By contrast, the model run with NCEP heat fluxes alone resulted in a mixed layer that was more than 1000 m shallower, and the best-estimate heat fluxes without tip jets produced a 500-m-shallower mixed layer. This result adds to the growing body of results supporting the hypothesis that deep convection in the central Irminger Sea may occur during high-NAO winters, and that Greenland tip jet events are a dominant driver of such overturning.

c. *Sensitivity*

To assess the robustness of the model–data comparison of mixed layer depths presented above, we applied a second mixed layer model and also considered an alternate bulk formula parameterization for the heat fluxes. The mixed layer model was that of Wang (2003), which is based on an empirical formula for the ratio of entrainment buoyancy flux to the surface buoyancy flux as a function of the natural Rossby number,[5] which acts as a measure of the constraint on deep convection by the earth's rotation. Using this model with a time step of 1 h (with interpolated fluxes) and a depth resolution of 0.1 m, the final depth of convection at the end of winter was about the same as for the PWP model for both the winters of 0203 (50 m shallower) and 0304 (30 m shallower). For the winter of 9495, convection in the Wang (2003) model reached a bit deeper (by 90 m). In the nonrotating limit ($R_0 \rightarrow \infty$ and the ratio of entrainment buoyancy flux to surface buoyancy flux becomes constant), the model predicted mixed layers only marginally deeper than the other model runs (30, 20, and 60 m for the winters of 0203, 0304, and 9495, respectively). For the winters of 0203 and 0304 the majority of the time steps had Rossby numbers greater than 0.5, and large differences between rotating and nonrotating convection were not expected. For the winter of 9495 the mean Rossby number was 0.5 and 44% of the timesteps exceeded this value, resulting in a greater difference between the rotating and the nonrotating cases (albeit still marginal, in terms of percentage).

The bulk formula of Renfrew et al. (2002), whose algorithm is essentially that of Smith (1988) with updated neutral exchange coefficients from DeCosmo et al. (1996), was used to produce a second set of best-estimate heat fluxes at the mooring site. The correlation between the two best-estimate heat flux time series was greater than 0.99, and the mean values differed by less than 6%. The main difference occurred during high-wind events, where the Fairall et al. (2003) fluxes exceeded the Renfrew et al. (2002) fluxes. The resulting

[5] The natural Rossby number is defined as $R_0 = [(B_0/f)^{1/2}]/fh$, where B_0 is the surface buoyancy flux, f is the Coriolis parameter, and h is the depth of the mixed layer.

final mixed layers when applied to the PWP model were similar for the heat flux time series from both bulk formulas, and both produced significantly shallower mixed layers when the tip jets were removed from the forcing. Our best-estimate heat fluxes were also compared with the heat flux product of Yu and Weller (2007) interpolated to the mooring site for the winters of 0203 and 0304. Differences occurred mainly during tip jet events, as their daily one-degree fluxes do not resolve the high time- and spatial-scale events properly. The heat flux time series had correlations of 0.77 and 0.71 and mean differences of 3 and 2 W m^{-2} for each winter, respectively.

In summary, the application of an alternative bulk heat flux formula and a 1D mixed layer model resulted in minor quantitative differences compared with the preceding results, and the conclusions of section 5b remain unchanged.

6. Summary and conclusions

Pickart et al. (2003a) cast doubt on the "Labrador Sea–centric" view that the Labrador Basin is the sole location of LSW formation. They showed, with the exception of atmospheric forcing, that all of the conditions required for deep convection are satisfied also in the Irminger Sea. Along with other studies (e.g., Bacon et al. 2003; Straneo et al. 2003), indirect evidence of deep convection occurring east of Greenland was presented. Pickart et al. (2003b) identified a mechanism capable of enhancing the atmospheric forcing over the southern Irminger Sea, in the form of strong, intermittent wind events called Greenland tip jets, which regularly form when low pressure systems occupy the area between Greenland and Iceland.

A moored profiler was deployed in the Irminger Sea east of Greenland under the expected path of the tip jet from 2002–04. The NAO index during this period was generally low. Mixed layers deeper than 60 m were observed between November and May, with final mixed layer depths of about 400 and 300 m reached by the end of the convective season for the winters of 0203 and 0304, respectively. Composite averages of the tip jet events for each winter, readily detected using an EOF approach, portray the tip jet as an intense, short-lived phenomenon, with peak wind speeds exceeding 25 m s^{-1}. The events occur when the parent cyclone is located to the northeast of Cape Farewell, causing enhanced SLP gradients to the east of the tip of Greenland, and increased ocean-to-atmosphere heat flux.

The effect of the tip jets on the evolution of the mixed layer was investigated with a 1D mixed layer model (Price et al. 1986). Best-estimate turbulent heat fluxes based on time series of wind, humidity, and air and sea surface temperatures from various sources and calibrated using data from a meteorological buoy at the mooring site were computed using the bulk formula of Fairall et al. (2003). These heat flux time series were used to force the model, and the results agreed well with the envelope of the mixed layer deepening deduced from the moored profiler observations for both winters. Removal of the 11 robust tip jet events from the heat flux time series of the first winter resulted in a 20% shallower mixed layer, indicating that the integrated effect of these storms contributed significantly to the deepening of the mixed layer. To assess the effects of tip jets during a high-NAO winter, the model was applied to the winter of 9495. At the end of this winter, the model mixed layer depth had exceeded 1700 m, which is consistent with hydrographic measurements from the following summer (Pickart et al. 2003a). This suggests that deep convection can take place in the southwest Irminger Sea under more favorable conditions.

Acknowledgments. The authors thank John Toole, Paula Fratantoni, and Anna Nikolopoulos for very helpful discussions regarding the processing and calibration of the moored profiler instruments. The Matlab version of the PWP model was kindly provided by Tom Farrar, and the OAFlux heat flux product by Lisan Yu. We acknowledge the NOAA Climate Diagnostics Center for the NCEP reanalysis data (www.cdc.noaa.gov). QuikSCAT data are produced by Remote Sensing Systems and sponsored by the NASA Ocean Vector Winds Science Team (www.remss.com). Finally, we thank Fiamma Straneo, Tom Farrar, and three anonymous reviewers for helpful comments on the manuscript. KV and RP were supported by National Science Foundation Grant OCE-0450658. GWKM was supported by the Canadian Foundation for Climate and Atmospheric Sciences. MHR was supported by the Nordic Council of Ministers (West-Nordic Ocean Climate).

REFERENCES

Bacon, S., W. J. Gould, and Y. Jia, 2003: Open-ocean convection in the Irminger Sea. *Geophys. Res. Lett.,* **30,** 1246, doi:10.1029/2002GL016271.

Bakalian, F., S. Hameed, and R. Pickart, 2007: Influence of the Icelandic Low latitude on the frequency of Greenland tip jet events: Implications for Irminger Sea convection. *J. Geophys. Res.,* **112,** C04020, doi:10.1029/2006JC003807.

Bramson, L., 1997: Air-sea interactions and deep convection in the Labrador Sea. M.S. thesis, Department of Oceanography, Naval Postgraduate School, 76 pp.

Centurioni, L. R., and W. J. Gould, 2004: Winter conditions in the Irminger Sea observed with profiling floats. *J. Mar. Res.,* **62,** 313–336.

Chelton, D. B., M. G. Schlax, M. H. Freilich, and R. F. Milliff, 2004: Satellite measurements reveal persistent small-scale features in ocean winds. *Science,* **303,** 978–983.

Clarke, R. A., and J.-C. Gascard, 1983: The formation of Labrador Sea water. Part I: Large-scale processes. *J. Phys. Oceanogr.,* **13,** 1764–1778.

DeCosmo, J., K. B. Katsaros, S. D. Smith, R. J. Anderson, W. A. Oost, K. Bumke, and H. Chadwick, 1996: Air-sea exchange of water vapor and sensible heat: The Humidity Exchange Over the Sea (HEXOS) results. *J. Geophys. Res.,* **101,** 12 001–12 016.

Dickson, R., and J. Brown, 1994: The production of North Atlantic Deep Water: Sources, rates, and pathways. *J. Geophys. Res.,* **99,** 12 319–12 342.

——, J. Lazier, J. Meincke, P. Rhines, and J. Swift, 1996: Long-term coordinated changes in the convective activity of the North Atlantic. *Prog. Oceanogr.,* **38,** 241–295.

Doherty, K. W., D. E. Frye, S. P. Liberatore, and J. M. Toole, 1999: A moored profiling instrument. *J. Atmos. Oceanic Technol.,* **16,** 1816–1829.

Doyle, J. D., and M. A. Shapiro, 1999: Flow response to large-scale topography: The Greenland tip jet. *Tellus,* **51A,** 728–748.

Fairall, C. W., E. F. Bradley, J. E. Hare, A. A. Grachev, and J. B. Edson, 2003: Bulk parameterization of air–sea fluxes: Updates and verification for the COARE algorithm. *J. Climate,* **16,** 571–591.

Falina, A., A. Sarafanov, and A. Sokov, 2007: Variability and renewal of Labrador Sea Water in the Irminger Basin in 1991–2004. *J. Geophys. Res.,* **112,** C01006, doi:10.1029/2005JC003348.

Fratantoni, D. M., 2001: North Atlantic surface circulation during the 1990's observed with satellite-tracked drifters. *J. Geophys. Res.,* **106,** 22 067–22 094.

Hoskins, B. J., and K. I. Hodges, 2002: New perspectives on the Northern Hemisphere winter storm tracks. *J. Atmos. Sci.,* **59,** 1041–1061.

Kalnay, E., and Coauthors, 1996: The NCEP/NCAR 40-Year Reanalysis Project. *Bull. Amer. Meteor. Soc.,* **77,** 437–471.

Lab Sea Group, 1998: The Labrador Sea deep convection experiment. *Bull. Amer. Meteor. Soc.,* **79,** 2033–2058.

Lavender, K., R. Davis, and W. Owens, 2000: Mid-depth recirculation observed in the interior Labrador and Irminger seas by direct velocity measurements. *Nature,* **407,** 66–69.

——, W. Owens, and R. Davis, 2005: The mid-depth circulation of the subpolar North Atlantic Ocean as measured by subsurface floats. *Deep-Sea Res. I,* **52,** 767–785.

Lazier, J., R. Hendry, A. Clarke, I. Yashayaev, and P. Rhines, 2002: Convection and restratification in the Labrador Sea, 1990–2000. *Deep-Sea Res. I,* **49,** 1819–1835.

Lilly, J. M., P. B. Rhines, M. Visbeck, R. Davis, J. Lazier, F. Schott, and D. Farmer, 1999: Observing deep convection in the Labrador Sea during winter 1994/95. *J. Phys. Oceanogr.,* **29,** 2065–2098.

Lorbacher, K., D. Dommenget, P. P. Niiler, and A. Köhl, 2006: Ocean mixed layer depth: A subsurface proxy of ocean-atmosphere variability. *J. Geophys. Res.,* **111,** C07010, doi:10.1029/2003JC002157.

Marshall, J., and F. Schott, 1999: Open-ocean convection: Observations, theory, and models. *Rev. Geophys.,* **37,** 1–64.

McCartney, M., 1992: Recirculating components to the deep boundary current of the northern North Atlantic. *Prog. Oceanogr.,* **29,** 283–383.

Moore, G. W. K., 2003: Gale force winds over the Irminger Sea to the east of Cape Farewell, Greenland. *Geophys. Res. Lett.,* **30,** 1894, doi:10.1029/2003GL018012.

——, and I. A. Renfrew, 2002: An assessment of the surface turbulent heat fluxes from the NCEP–NCAR reanalysis over the western boundary currents. *J. Climate,* **15,** 2020–2037.

——, and ——, 2005: Tip jets and barrier winds: A QuikSCAT climatology of high wind speed events around Greenland. *J. Climate,* **18,** 3713–3725.

Petersen, G. N., H. Ólafsson, and J. E. Kristjánsson, 2003: Flow in the lee of idealized mountains and Greenland. *J. Atmos. Sci.,* **60,** 2183–2195.

Pickart, R. S., D. J. Torres, and R. A. Clarke, 2002: Hydrography of the Labrador Sea during active convection. *J. Phys. Oceanogr.,* **32,** 428–457.

——, F. Straneo, and G. W. K. Moore, 2003a: Is Labrador Sea Water formed in the Irminger basin? *Deep-Sea Res. I,* **50,** 23–52.

——, M. A. Spall, M. H. Ribergaard, G. W. K. Moore, and R. F. Milliff, 2003b: Deep convection in the Irminger Sea forced by the Greenland tip jet. *Nature,* **424,** 152–156.

Price, J. F., R. A. Weller, and R. Pinkel, 1986: Diurnal cycling: Observations and models of the upper ocean response to diurnal heating, cooling, and wind mixing. *J. Geophys. Res.,* **91,** 8411–8427.

Renfrew, I. A., G. W. K. Moore, P. S. Guest, and K. Bumke, 2002: A comparison of surface layer and surface turbulent flux observations over the Labrador Sea with ECMWF analyses and NCEP reanalyses. *J. Phys. Oceanogr.,* **32,** 383–400.

Schmitz, W. J., Jr., and M. S. McCartney, 1993: On the North Atlantic circulation. *Rev. Geophys.,* **31,** 29–50.

Schott, F., M. Visbeck, and J. Fischer, 1993: Observations of vertical currents and convection in the central Greenland Sea during the winter of 1988–1989. *J. Geophys. Res.,* **98,** 14 401–14 422.

——, ——, U. Send, J. Fischer, L. Stramma, and Y. Desaubies, 1996: Observations of deep convection in the Gulf of Lions, northern Mediterranean, during the winter of 1991/92. *J. Phys. Oceanogr.,* **26,** 505–524.

Serreze, M. C., F. Carse, R. G. Barry, and J. C. Rogers, 1997: Icelandic low cyclone activity: Climatological features, linkages with the NAO, and relationships with recent changes in the Northern Hemisphere circulation. *J. Climate,* **10,** 453–464.

Smith, S., 1988: Coefficients for sea surface wind stress, heat flux, and wind profiles as a function of wind speed and temperature. *J. Geophys. Res.,* **93,** 15 467–15 472.

Spall, M. A., and R. S. Pickart, 2003: Wind-driven recirculations and exchange in the Labrador and Irminger Seas. *J. Phys. Oceanogr.,* **33,** 1829–1845.

Straneo, F., R. S. Pickart, and K. Lavender, 2003: Spreading of Labrador Sea water: An advective-diffusive study based on Lagrangian data. *Deep-Sea Res. I,* **50,** 701–719.

Sverdrup, H. U., M. W. Johnson, and R. H. Fleming, 1942: *The Oceans: Their Physics, Chemistry, and General Biology.* Prentice-Hall, 1087 pp.

Sy, A., M. Rhein, J. Lazier, K. Koltermann, J. Meincke, A. Putzka, and M. Bersch, 1997: Surprisingly rapid spreading of newly formed intermediate waters across the North Atlantic Ocean. *Nature,* **386,** 675–679.

Talley, L. D., 2003: Shallow, intermediate, and deep overturning components of the global heat budget. *J. Phys. Oceanogr.,* **33,** 530–560.

——, and M. S. McCartney, 1982: Distribution and circulation of Labrador Sea water. *J. Phys. Oceanogr.,* **12,** 1189–1205.

Toole, J. M., K. W. Doherty, D. E. Frye, and S. P. Liberatore, 1999: Velocity measurements from a moored profiling instrument. *Proc. IEEE Sixth Working Conf. on Current Measurement,* San Diego, CA, IEEE, 144–149.

Tsukernik, M., D. N. Kindig, and M. C. Serreze, 2007: Characteristics of winter cyclone activity in the northern North Atlantic: Insights from observations and regional modeling. *J. Geophys. Res.,* **112,** D03101, doi:10.1029/2006JD007184.

Våge, K., 2006: Winter mixed layer development in the central Irminger Sea: The effect of strong, intermittent wind events. M.S. thesis, Joint Program in Physical Oceanography, Woods Hole Oceanographic Institute and Massachusetts Institute of Technology, 79 pp. [Available online at http://www.whoi.edu/science/PO/pickart/Online_pubs_main.htm.]

Vautard, R., 1990: Multiple weather regimes over the North Atlantic: Analysis of precursors and successors. *Mon. Wea. Rev.,* **118,** 2056–2081.

Wang, D., 2003: Entrainment laws and a bulk mixed layer model of rotating convection derived from large-eddy simulations. *Geophys. Res. Lett.,* **30,** 1929, doi:10.1029/2003GL017869.

Wentz, F., D. Smith, C. Mears, and C. Gentemann, 2001: Advanced algorithms for QuikScat and SeaWinds/AMSR. *Proc. Int. Geosci. Remote Sens. Symp. (IGARSS'01),* Sydney, Australia, IEEE, 1079–1081.

Yu, L., and R. A. Weller, 2007: Objectively analyzed air–sea heat fluxes for the global ice-free oceans (1981–2005). *Bull. Amer. Meteor. Soc.,* **88,** 527–539.